Time-Lapse Electrical Resistivity Tomography Applied to Cave Sustainability (Barbados) and Groundwater Exploration (Saint Lucia)

by

Yulia Agramakova

B.S. Geophysics

Moscow State University, 2005

SUBMITTED TO THE DEPARTMENT OF EARTH, ATMOSPHERIC, AND PLANETARY SCIENCES IN PARTIAL FULFILLMENT OF THE REQUIREMENTS FOR THE DEGREE

OF

MASTER OF SCIENCE IN GEOPHYSICS

AT THE

MASSACHUSETTS INSTITUTE OF TECHNOLOGY

FEBRUARY 2011

Signature of Author: ___

Department of Earth, Atmospheric, and Planetary Sciences

February 4, 2011

Certified by: _

Frank Dale Morgan

Professor of Geophysics

Thesis Supervisor

Accepted by: ____

Maria T. Zuber

Head of the Department of Earth, Atmospheric, and Planetary Sciences

Time-Lapse Electrical Resistivity Tomography Applied to Cave Sustainability (Barbados) and Groundwater Exploration (Saint Lucia)

by

Yulia Agramakova

Submitted to the Department of Earth, Atmospheric, and Planetary Science
on May 21, 2010, in Partial Fulfillment of the Requirements
for the Degree of Master of Science in Geophysics

Abstract

In this work we apply the method of two-dimensional time-lapse electrical resistivity tomography (2D time-lapse ERT) for two different problems. In the first problem, we monitor the structural stability of the roof of the Great Hall cavern in the Harrison's cave system, Barbados. We present an interpretation and comparison of two sets of resistivity data collected over the Great Hall: one set collected by us in 2010, the other in 1996. Our results show that fracturing and degradation had progressed since 1996, indicating a gradual weakening of the structural stability of the roof of the Great Hall cavern. In the second problem, we conduct 2D ERT surveys during dry and rainy seasons to evaluate the potential and feasibility of groundwater exploration next to the Thomazo River in the Fond D'Or watershed in Saint Lucia. Interpretation of the ERT data sets reveals a lens of a porous rock that has a high potential to be a productive aquifer. We use the ERT time-lapse approach to evaluate the change in water content between dry and wet seasons in the potential aquifer.

Thesis Supervisor: Frank Dale Morgan

Title: Professor of Geophysics

Table of Contents

List of Figures

List of Tables

Acknowledgements

First of all I would like to thank my advisor, Prof. Frank Dale Morgan, for his guidance, advice and encouragement throughout my work. He guided me in this research with unique patience and remarkable insight. It is my great fortune to be his student.

I also thank Prof. Nafi Toksöz and Dr. Michael Fehler for accepting to be on the defense committee and for their useful comments about my work. I gratefully acknowledge the support from Theodore R. Madden Graduate Fellowship in Geophysics and Chevron-MIT Energy Fellowship. I am thankful to the governments of St. Lucia and Barbados for sponsoring our field trips.

There are many people who went with me to the field trips to Barbados and St.Lucia and helped to collect the data. I am very thankful to all of them including Cornelius Isaac, Ananias Verneuil, Phil Reppert, Nasruddin Nazerali, Fred Pearce, Andrey Shabelansky, Bongani Mashele, Mirna Slim, Rachel Zucker, Alejandra Quintanilla-Terminel, Diego Concha, Katie Pesce, Anna Brunner, Rachel Bowens-Rubin, Clarion Hess, Sid Creutz. I would like to specially thank my advisor, Prof. Frank Dale Morgan, for collecting IP data and the resistivity data set in St.Lucia during the wet season.

I am grateful to John Sogade and Darrell Coles for their help with the resistivity inversion code. I am indebted to Ruel Jerry and especially to David Forney for their time and effort in proofreading my thesis.

I give my thanks to my group mates Nasruddin Nazerali, Bongani Mashele and Hussam Busfar for their company, support and interesting discussion during our group meetings. Special thanks go to Nasruddin Nazerali who was not only my office mate for 2.5 years but is also my good friend. I cherish the friendship of Abdulaziz AlMuhaidib, Sudhish Kumar Bakku, Diego Concha, Xinding Fang, Junlin Li, Gabi Melo, Fred Priece, Mirna Slim, Andrey Shabelansky and many others at MIT.

Finally, I would like to thank my husband, Vladimir, my family and my best friend Lyudmila for all their love and support.

Introduction

Electrical resistivity tomography (ERT) is one of the main geophysical techniques in near surface investigations. ERT allows for the determination of the resistivity distribution of the subsurface within the framework of two or three dimensional models. The ERT method can be applied to a wide range of engineering, environmental, archeological and hydrogeological problems.

In recent years, the ERT technique has been applied to address the numerous engineering problems that include, but are not limited to, studying the internal structure and depth of landslides [Lapenna et al., 2003; Niesner and Weidinger, 2008; Lebourg et al., 2010]; investigation of the slope stability [Hack, 2000; Suzuki and Higashi, 2001; Friedel et al., 2006]; detection of faults and fractured zones [Gelis, 2010]; investigation of karst terrains [Roth et al., 2002; Szalai et al, 2002; Nyquist, 2007; Valois et al, 2010] delineation of cave systems [Morgan and Wharton, 1996; Shi ,1998; Panek, 2010] and their stability [Leucci and Giorgi, 2005].

In hydrogeological and environmental research, the main focus of ERT investigations is on the detection of the presence of water or the movement of water and contaminants. The ERT technique was successfully applied to map solute transport in the subsurface [Kemna et al., 2002;]; to detect leakage from an underground storage tank [Daily et al., 2004]; and to study the water movement in vadose (unsaturated) zones of the subsurface [Daily et al., 1992].

The traditional ERT technique provides only the static image of the electrical properties of the subsurface. The electrical properties of rocks and soils depend on several factors such as the nature and amount of pore fluid, and the porosity of the rock matrix. These factors which determine the electrical properties of the subsurface can change with time causing a change of the resistivity distribution of the subsurface. Therefore, the utilization of the ERT method in the time-lapse mode opens new possibilities to study the changes of the electrical properties of the subsurface caused by different factors. ERT surveys are repeated over the same line at different times to study the changes of subsurface resistivity with time. In recent years, the time-lapse ERT method has been widely used in hydrogeological and environmental research to study the

flow of water through the vadose zone, to detect changes in the water table due to water extraction, and to monitor the flow of chemical pollutants and leakage from dams.

The changes in the subsurface resistivity can be determined from time-lapse field measurements by several methods. The straightforward approach is to independently invert the data sets from two time periods by using available inversion algorithms [Shi, 1998; Zhang et al., 1995]. Then the change in resistivity distributions can be obtained by simply subtracting the resistivity values pixel-by-pixel from two inversion models [Slater and Sandberg, 2000]. This approach is subject to a higher error and the final output may contain artifacts. The artifact can appear in the final image if, for example, one of the data sets has a higher noise level with the result that the images obtained by independent inversions will have a different resolution [Miller et al., 2008; Cassiani et al, 2005]. The other source of artifacts comes from the errors in the electrode positions between two time periods [Oldenborger et al., 2005] and the inversions themselves.

Another commonly used method in time-lapse inversion is the inversion of data differences. It had been shown by [Shi, 1998; Miller et al., 2008] that this approach is most sensitive to noise in the data; therefore, the information about the noise level in the data should be available and taken into consideration to obtain a reliable model of the resistivity changes.

An alternative approach to the data differences inversion is to use a ratio of the two data sets in the inversion algorithm. This method has the capability to resolve the small changes in resistivity in the subsurface [Cassiani et al., 2005; Daily et al., 1992].

Finally, a reference model can be incorporated into inversion of the data difference or ratio of two data sets. The inversion output of the initial data set can be used as a reference model [Loke 1999; LaBrecque and Yang, 2001]. This approach adds an additional constraint to the inversion solution which minimizes possible inversion artifacts. On the other hand, the final time-lapse image may be strongly dependent on the reference model used [Shi, 1998; Kim et al., 2009].

This work focuses on the application of time-lapse ERT for groundwater exploration in Saint Lucia and monitoring the structural stability of a large cavern in the show cave system in Barbados.

The resistivity data collected in Barbados with a difference in 14 years were inverted independently and compared in order to investigate if any significant changes in the cave's shape, size and overall porosity of the surrounding areas took place since the fist data set was collected.

The time-lapse approach was also applied to the data sets collected in Saint Lucia to evaluate the change in water content between dry and "rainy" seasons in the potential aquifer. To estimate the changes of water content and effective porosity a ratio of the independently inverted data sets was considered.

Inversion method

In both projects the same inversion algorithm were used to determine the subsurface distribution of the resistivity values.

The apparent resistivity values measured in the field are not equal to the true values of the resistivity in the subsurface. The only case when the measured resistivity represents the true subsurface resistivity is if the measurements were carried out over a homogenous half-space. Therefore, an inverse method is utilized to determine an image of the spatial resistivity variations. Both data sets were inverted using an inversion code developed in the Earth Resources Laboratory at MIT [Shi, 1998; Zhang et al., 1995].

The fundamental equation governing the direct current resistivity response is Ohm's low written in differential form as following:

$$\nabla\left(\frac{1}{\rho(\mathbf{x})}\nabla V(\mathbf{x})\right) = -I(\mathbf{x}) \qquad (1),$$

where $\rho(x)$ is resistivity distribution, V is electric potential at a point x(i, j, k) and I is current.

The transmission network analog technique developed by Madden [Madden, 1969; Madden, 1972] is applied to solve the equation (1) numerically. The basic idea is that the earth could be approximated by a network of nodes and impedance branches which are proportional to the model resistivity values. The voltage nodes V(i, j, k) are positioned at the center of the top face of each medium block. The impedance elements R_x, R_y and R_z

are defined on the network branches. This implies that the impedance elements R_x, R_y and R_z can be expressed though the grid spacing $\Delta x(i)$, $\Delta y(j)$, $\Delta z(k)$ in each dimension for a block (i, m, k) and the resistivity $\rho(x)$ of the block (i, j, k) [Zhang et al., 1995]. The voltage is defined in all nodes where as for a surface electrical resistivity tomography (ERT) the current sources could be placed in any surface nodes. For a general problem, a current source can be associated with any network nodes. Finally, if we apply Kirchhoff's current law to the network of impedances the following system of linear equations written in matrix form can be obtained:

$$Kv=s \qquad (2),$$

where v is vector consisting of the voltage values at each network nodes, s is the current source vector and K is the coefficient matrix defined by resistivity values of each block and the network block dimensions.

The goal of the inverse problem is to find a model m that would reproduce data *d* with a specified level of confidence. To achieve a stable and accurate solution and to overcome an inherent non-uniqueness of an inverse problem combined with the presence of the data errors we have to impose additional constraints. It is achieved by the use of Tikhonov regularization, where an objective function takes the following form:

$$\Psi(\boldsymbol{m}) = \|d - G(\boldsymbol{m})\|^2 + \tau\left\|L(\boldsymbol{m} - \boldsymbol{m_{ref}})\right\|^2 \qquad (3),$$

where G is the forward modeling operator, L denotes Laplacian operator, $\mathbf{m_{ref}}$ is a reference model, m is a current model and τ is a regularization parameter which controls a tradeoff between the influence of data misfit (first term in eq.3) and a stabilizing model objective function (second term in eq.3) in the inversion [Shi, 1998; Binley and Kemma, 2005].

The implementation of the minimization is accomplished by applying a nonlinear conjugate gradient algorithm with preconditioning described in detail in [Shi, 1998].

Part I: Time-Lapse ERT Technique Applied to Investigate the Structural Stability of the Great Hall Cavern in Harrison's Cave System, Barbados

Motivation

The delineation of the cave systems in the areas of karst development has always been a challenging problem due to their complex geometries. Many geophysical methods have been employed for investigation of a cave structure including electrical resistivity, ground penetrating radar, and seismic methods [Morgan and Wharton, 1996; Cardarelli et al., 2003; Nyquist et al., 2007; Abu-Shariah, 2009; Lazzari et al., 2010; Panek 2010]. Geophysical methods offer non-invasive approaches to obtain the information about the geometry of the subsurface structures on large scales. An additional advantage of these methods is the possibility of repeating them over time for monitoring purposes.

Contrary to geophysical methods, the direct technique such as drilling, with rock sampling, can be used to determine the physical properties of the in-situ rock and evaluate the extent of fracturing in the subsurface. However, the information from drilling cannot always be extrapolated to large areas. In the case of cave structure monitoring, drilling can damage the structural integrity of the cave which is a crucial factor when a residential area is located just above a cave system. In such situations, a geophysical survey is certainly preferable.

The structural stability of a cave depends on the presence of the fractures in the rock constituents of the cave and, in general, it is proportional to the thickness of the overburden and inversely proportional to the width of the cavern. Moreover, progressive cracking within the bed rock is considered to be one of the main causes of collapse in caves.

This work focuses on the use of electrical resistivity tomography (ERT) to monitor the structural integrity of the Great Hall cavern in the Harrison's cave system located in Barbados, and contains the interpretation and comparison of the resistivity data collected over the Great Hall with a time difference of 14 years.

The Harrison's cave in Barbados, West Indies (Fig. 1), has been a popular tourist attraction on the island for the last 30 years. One of the main areas of the Harrison's cave

system is a huge cavern, called "the Great Hall". A small village is located directly over the Great Hall. The presence of the village and the human activity in such close proximity to the Great Hall not only promote pollution to the fragile cave environment, but also, and more importantly, can lead to the collapse of the cave's roof which can put the lives of the village residents at risk.

To address the issues of the cave's structural stability, maintenance and future development it is important to have very accurate information about the size, shape and extent of the cave system. Therefore, in August of 1996, the geophysical group from MIT started their investigations over Harrison's cave to remotely map the underground cave structure by using different geophysical methods. After 14 years, in January 2010, the same geophysical methods were conducted again to map the Great Hall. The main objective was to see if there are any significant changes in the cave's shape, size and overall porosity of the surrounding areas, compared to the results from 1996. It is important to understand that a cave represents a potentially dynamic structural environment; therefore, continued and careful monitoring of the cave is essential to identify whether the fracturing in the cave is progressing.

Geology of the region

Barbados is a small island located in the most easterly part of the Caribbean sea (Fig.1). The island was formed by the gradual accretion of the oceanic sediments and tectonic uplifts caused by the Atlantic plate being pushed under the Caribbean plate resulting in an uneven uplift of the island. According to Mesolella, this uneven uplift probably has continued to the present time with the rate of elevation gain raging from 0.07 to 0.44 mm per year [Mesolella et al., 1970; Taylor and Mann, 1991].

About 85% of the exposed rock in Barbados is Pleistocene reef limestone. The remaining outcrop consists of Tertiary sedimentary rocks of marine origin (Fig.2) [6, 7, 8]. The island was tectonically uplifted in the Pleistocene and the coral reefs were formed around the island during the periods of eustatic high sea level stands [Mesolella et al., 1970]. The tectonic elevation of the coral reefs created a series of limestone terraces with

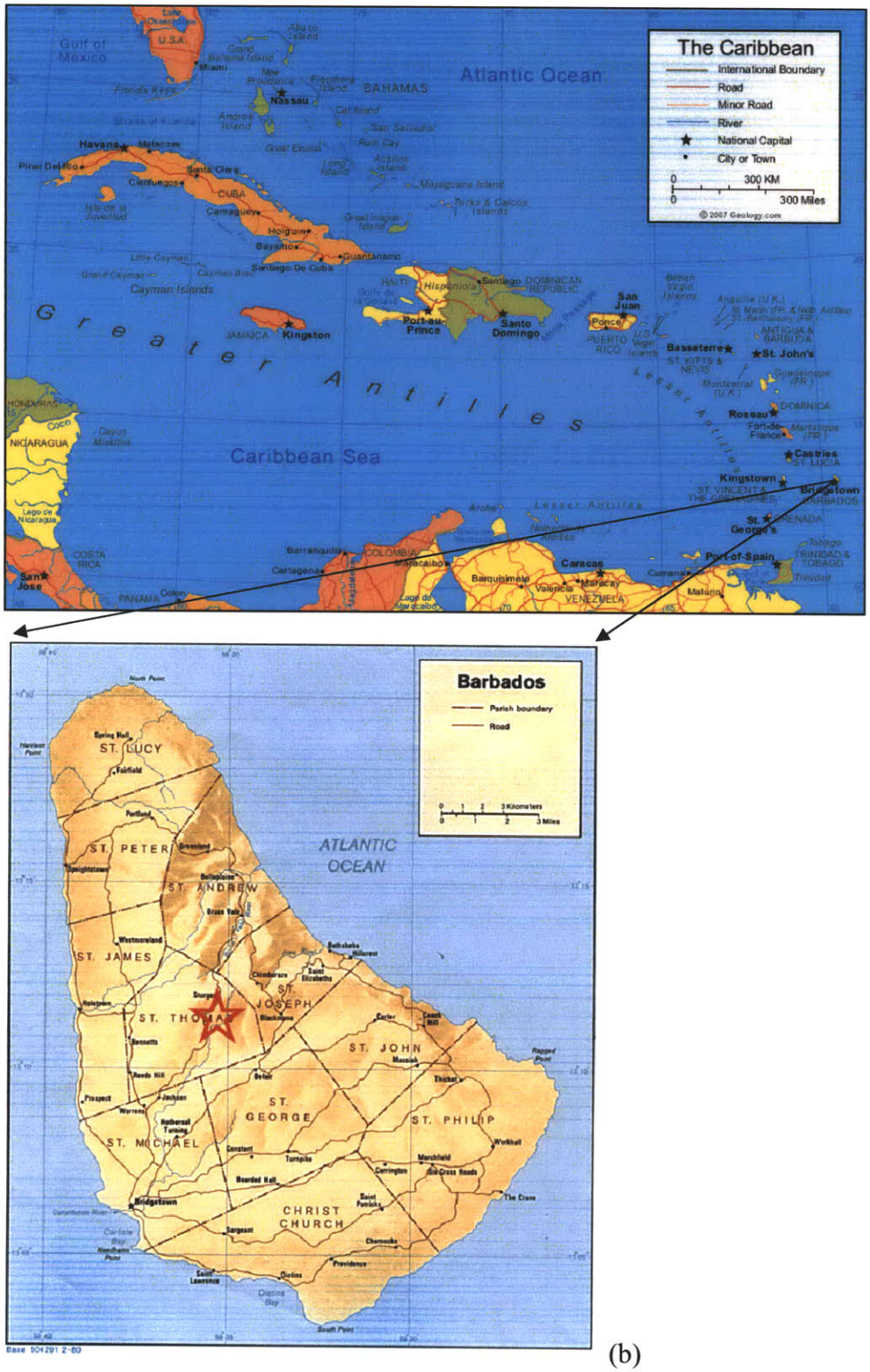

(a)

(b)

Figure 1. Geographical location of Barbados (a). Shaded areas on the zoomed image (b) represent the relief of the island. The location of the Harrison's cave system is marked by a red star (b)

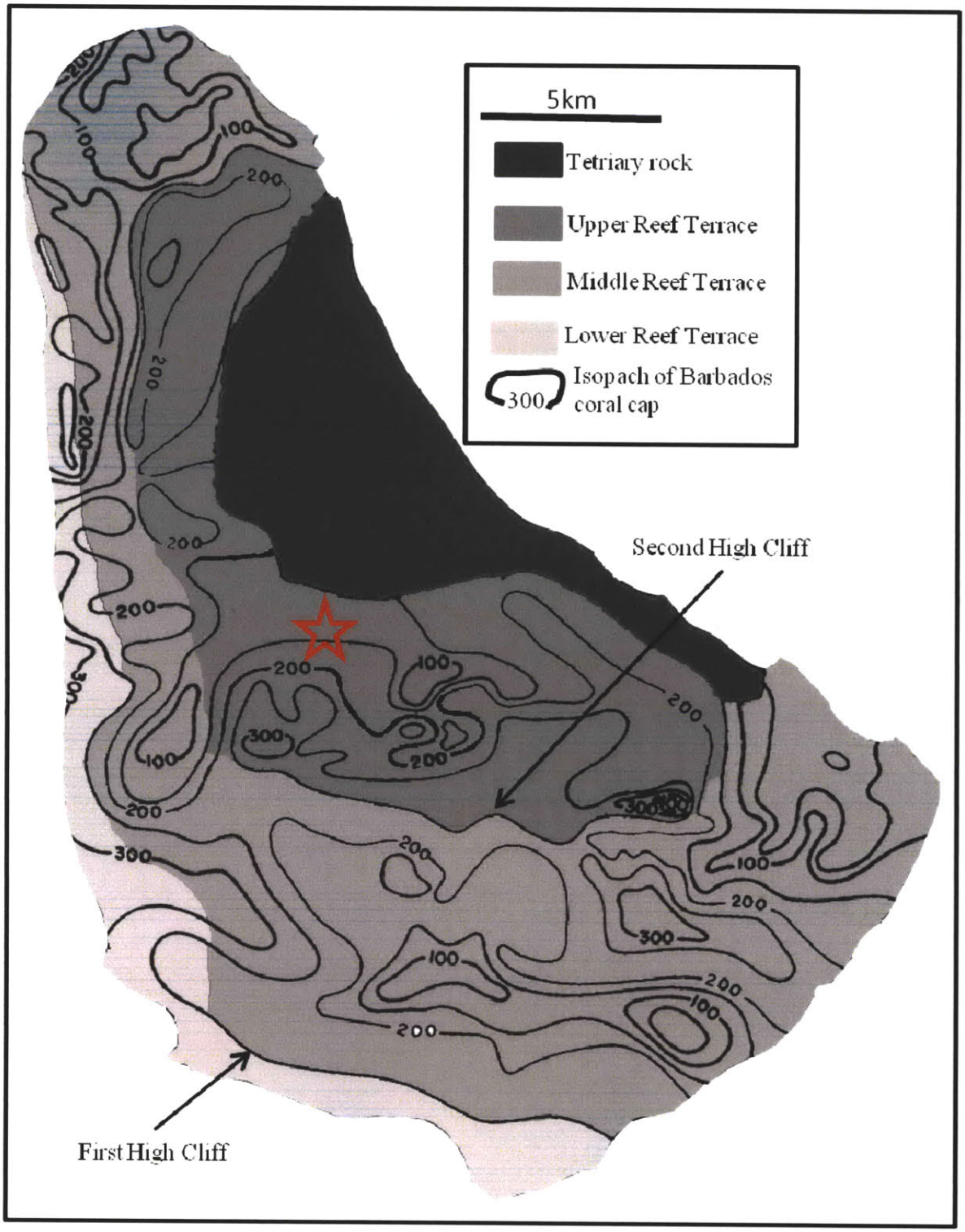

Figure 2. Areal distribution of major reef terraces on Barbados. Contour lines represent the thickness of the limestone deposits (contour line interval is 50 ft). The location of the Harrison's cave system is marked by a red star. Modified from fig. 2 and fig 5 of ref. [Mesolella et al., 1970].

the highest and oldest limestones in the center of Barbados (Fig.2). The coral limestone is extremely porous and permeable which is indicated by the almost total absence of streams on the limestone part of the island, and the presence of many cave systems which were created by dissolution processes in the coralline limestone [Donovan, 2005, Mesolella et al., 1970].

The study area (Fig. 1, 2) is located in the center of the island near the southern end of Welchman Hall Gully which, in fact, was formed when the cave roof collapsed due to tectonic uplifting of the island. The Gully contains numerous formations that could only be created inside a cave (Fig.3). An interesting fact is that the Harrison's cave is geologically connected to the Gully and could be entered from Welchman Hall.

Summary of the previous studies in Harrison's cave

The current chapter aims to summarize the results of all available studies regarding the safety conditions within the Great Hall cavern in the Harrison's cave.

The tunnel constructions and enlargement of the existing narrow passages were some of the main parts in the development of the caves for tourists. In total, about 700 m of Harrison's cave system were artificially altered to accommodate a tram tourist tour [Hobbs, 1994]. These operations disturbed the existing equilibrium in the rock masses and created a new stress pattern in the limestone. In that new structural environment, the newly developed stress could increase the rate of fracture development as the whole system tries to regain equilibrium. Consequently, monitoring the known and newly developed fractures as well as potentially hazardous areas in the cave should be a top-priority task.

Since 1981, when the development of Harrison's cave was finished and the cave was opened for public viewing, a team of speleologists from the USA National Speleological Foundation (NSF) examined the cave structural stability by visual inspection twice, in 1986 and 1994. The visual examination in 1986 did not notice any significant fractures on the roof or walls of the Great Hall, whereas after 8 years, in 1994, a potentially unsafe area was detected. At floor level in the Great Hall, a slab of rock was possibly separated from the main wall by a series of clay layers. These layers of clay

Figure 3. Photograph showing the paleostalactite: an evidence of a cave collapse in the past (credit: Clarion Hess)

were interpreted as a zone of tensile weakness [Hobbs, 1994]. In the other caverns of the Harrison's cave system the NSF team observed several stress-release fractures developed as a response to the tunnel construction. Most of these fractures occurred near the intersections between natural and artificially enlarged parts of the cave and tend to be parallel to the tunnel wall. The NSF team recommended that any kind of fractures should be subject to a regular monitoring by visual means and/or direct or remote methods [Hobbs, 1994].

Following the suggestions of the NSF team about the monitoring of the stability of the cave, the group of researchers from MIT and University of West Indies conducted an extensive geophysical survey to delineate the major caverns and passages in the cave and evaluate their stability [Morgan and Wharton, 1996; Morgan et al., 2007]. Among the geophysical methods performed in 1996 were electrical resistivity tomography (ERT), ground penetration radar, seismic and gravity measurements. The area where the geophysical methods were carried out is shown on Fig. 4. Integrated interpretation of the data measured by the geophysical methods revealed a zone of high porosity in the overburden over the Great Hall and estimated the thickness of the bedrock over the Great Hall in the range between 20 – 25 meters [Morgan and Wharton, 1996]. In addition, the visual inspection of the cliff area at the Scenic Path (see the red dotted circle on Fig. 4) discovered large, to the extent of 0.3 m, vertical fractures. It suggests that similar fractures could be developed in the cave. If these fractures are coupled with the zone of high porosity then it would point out that bedrock over the Great Hall is weak [Morgan and Wharton, 1996; Shi, 1998]. As a main recommendation, the detailed subsurface imaging beneath the entire village of Allen View was proposed. The reason the Great Hall area obtained so much attention is that the ratio of the overburden thickness to the cave width is not large enough. As this ratio becomes smaller due to repeated roof collapses, the chance of a total roof collapse in the cave becomes higher. Furthermore, increased porosity and fracturing in the roof will lead to reduced tensile strength and end in catastrophic collapse.

To address the issues of roof stability in the caves and determine the possible scenarios of expansion of the show cave, AXYS Environmental Consulting performed

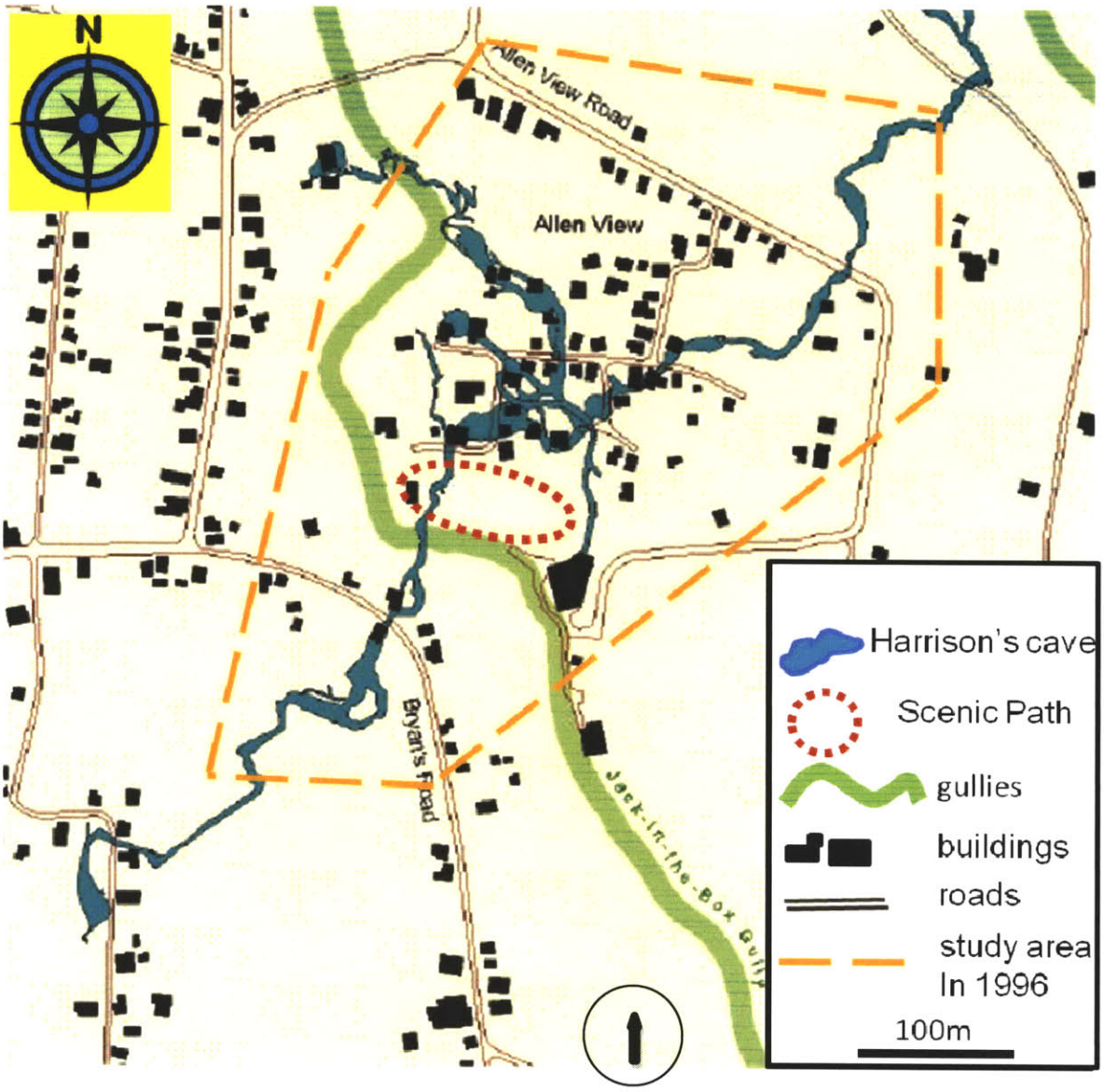

Figure 4 Footprint of the Harrison's cave system on the street map of the Allen View village. Dashed yellow line outlines the area where the geophysical investigations were conducted by MIT team. Black arrow points north. Modified from fig. 13 of ref. [AXIS report, 2000]

their investigations in 1998. They obtained the new estimations of the stop heights in the Great Hall and the overburden thickness [AXYS report, 2000]. The measurements of the overburden thickness are summarized in Table 1. As a comparison, the thickness data obtained in the Great Hall by NSF in 1994 are added to the Table 1.

	MIT, 2001	AXIS, 1998	NSF, 1994
West end of Great Hall	NA	36 m	27 m
Center of Great Hall	38 m	35.4 m	25 m

Table 1. Measurements of overburden thickness (data from ref. [AXYS report, 2000])

The main conclusion made by the AXIS group is that the occurrences of a collapse and rock fall have a very small probability in the Harrison's cave in general and in the Great Hall cavern in particular. At the same time it was pointed out that the concern about the weakness of the bedrock over the Great Hall cavern arising from the preliminary geophysical imaging requires further investigation and confirmation [AXYS report, 2000]. Therefore, they recommended repeating the geophysical imaging of the rock structure above the Great Hall to outline the faults and fractures in the vicinity of this cavern.

In 2001 and 2003, a group from MIT continued to work at the Harrison's cave inspecting the roof fractures, measuring the roof thickness in the Great Hall and running the numerical simulation of the stress pattern in the Great Hall under different scenarios [Morgan et al., 2007].

Because of some discrepancies between the overburden thickness over the Great Hall obtained by NSF and AXIS the measurements of the cave roof thickness in the Great Hall were repeated by MIT in 2001 and revealed the number 38 m which is consistent with the value of 35.4m determined by AXIS group (see Table 1) but differs a lot from the estimates by geophysical methods which give the range of roof thickness 20 – 25 m [15]. The most likely explanation of this discrepancy is the following. The thickness of

the roof in the Great Hall is indeed around 35 m; however, at a depth of 20 to 25 m from the surface a section of partially dislodged limestone is present. Therefore, if air fills in between the roof and the dislodged portion, it could lead to a situation where the geophysical methods detect the depth to the dislodged part in the roof rather than the actual cave roof thickness (Fig. 5) [Morgan et al., 2007].

In 2003, the research group from MIT detected three large fractures on the ceiling during the visual inspection inside the Great Hall [Morgan et al., 2007]. These fractures run across the ceiling width and are almost parallel to each other (see the sketch in Fig. 6). Taking into account the equidistant spacing and similar orientation (along north-south axis, ~340-350°) of these fractures, they most likely have developed as a result of stress release along the length of Great Hall [Morgan et al., 2007]. Worthy of note, the NSF listed the stress-release fracture as one of the potential reasons for roof collapse [Hobbs, 1994].

Based on the analysis of the strike angles of these fractures and the neighboring gullies the research team from MIT proposed an interesting hypothesis explaining the mechanism responsible for the development of these fractures. It can be seen in Fig.6 that the orientation of the fractures is nearly parallel to the strike angle (~340°) of nearby Welchman and Jack-in-the-Box gullies. MIT team hypothesized that the orientation of the gullies reflects the regional strain caused by uneven uplift of the island as the Atlantic plate subducts beneath the Caribbean Plate [Morgan et al., 2007]. Therefore, it is possible that regional strain promotes fracture development in the roof of the Great Hall and everywhere else. If this assumption is valid then the ceiling of the Great Hall along the East-West direction undergoes tensile stress which would pull the ceiling apart (Fig. 7) [Morgan et al., 2007].

As a result of these observations, the MIT team proposed drilling a borehole for sampling of the overburden material, and placing in the borehole a device that will detect and monitor small changes in the strain or deformation of the cave roof.

In January 2010, a group from MIT conducted the same geophysical survey again to map the Great Hall. The main objective was to see if there were any significant changes in the cave's shape, size and overall porosity of the surrounding areas compared

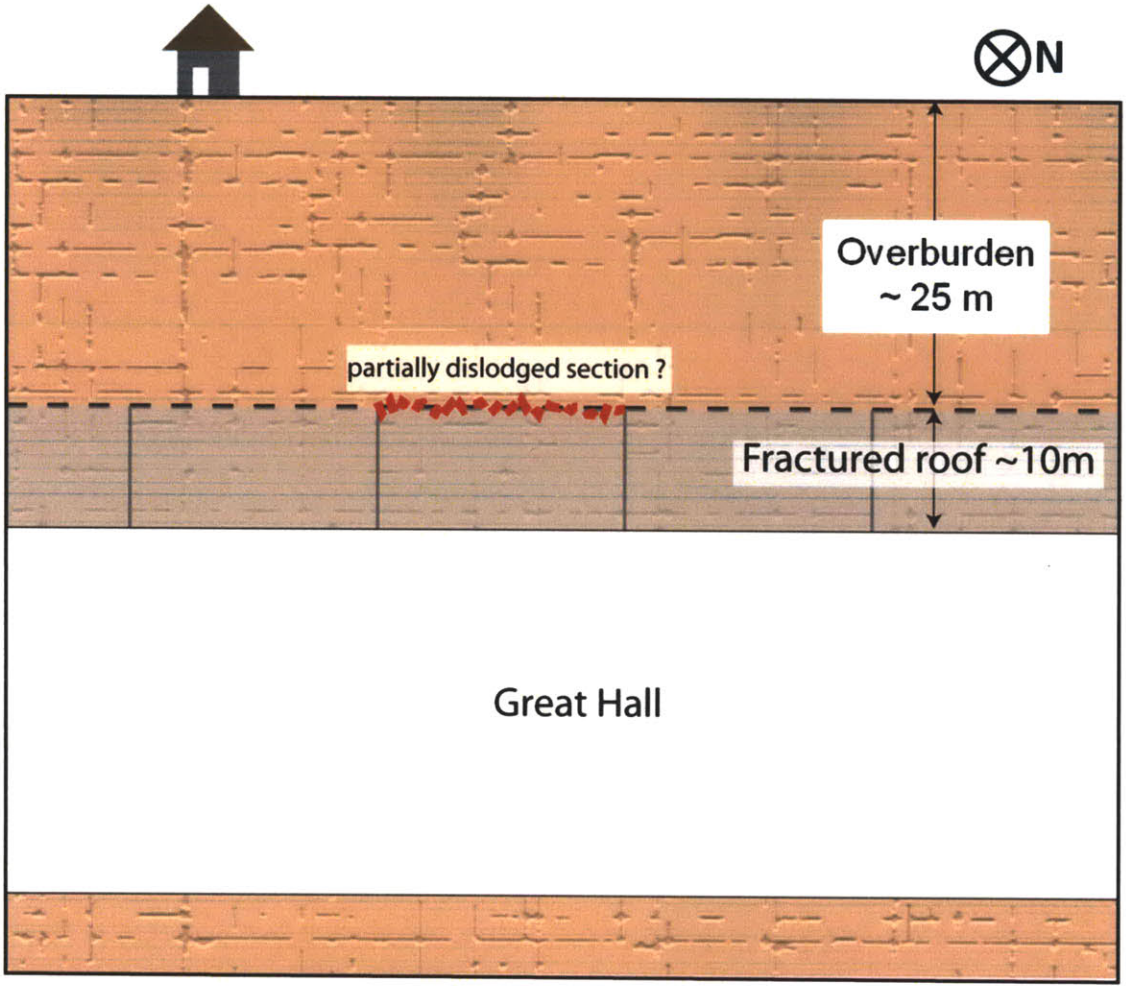

Figure 5. Diagram of the Great Hall roof and overburden. Modified from fig. 1 of ref. [Morgan et al., 2007]

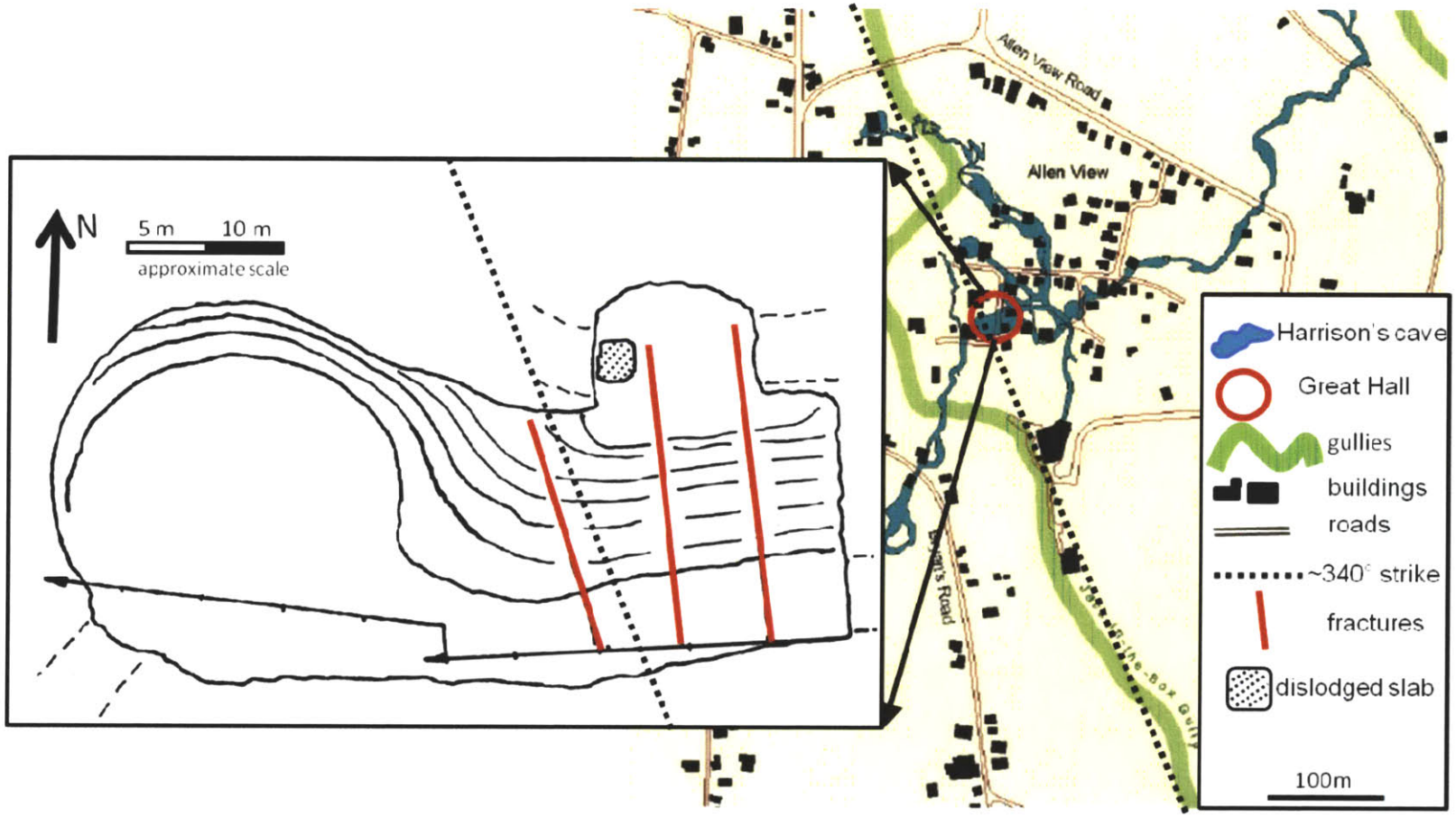

(a) (b)

Figure 6. (a) Plan view of the three large fractures observed in the Lower Great Hall ceiling (modified from fig.3.2.1. of ref [Morgan et al., 2007]); (b) plan view of the Allen View Village. Thick green line indicates the locations of the Welchman Hall Gully and Jack-in-the-Box Gully. Red circle outlines the location of the Great Hall. Notice that the strike of shown gullies is almost parallel to the fractures observed in the roof of the Great Hall. (modified from ref. [AXIS report, 2000]).

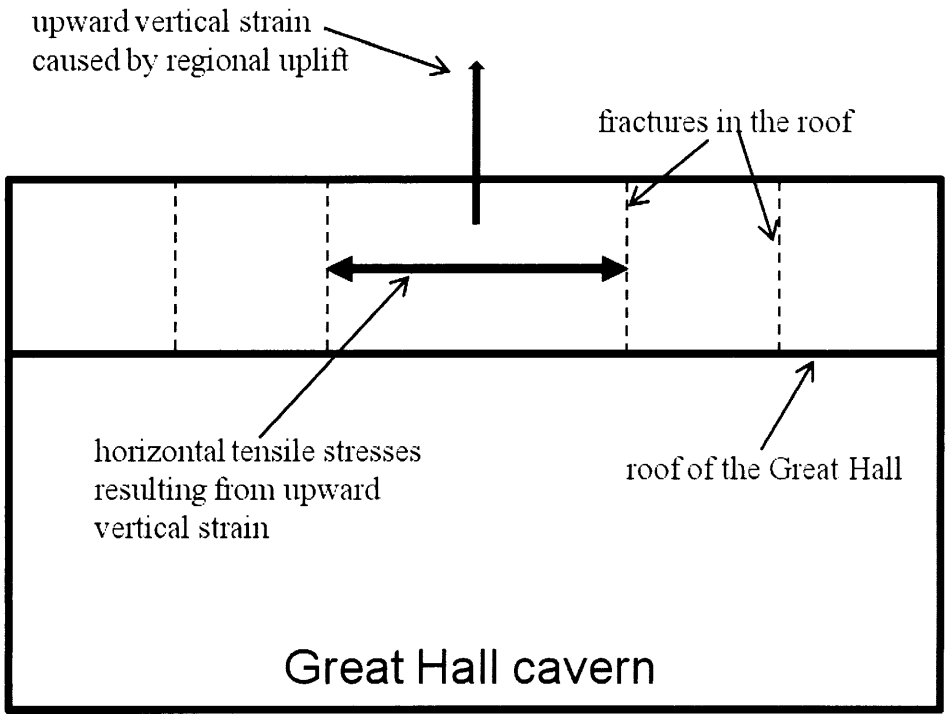

Figure 7. Cartoon of the primary upward strain and the horizontal stresses hypothesized to be working along the long dimension of the Great Hall cavern. The tensile strain caused by uneven regional uplift is a tenable explanation for the fractures observed in the roof of the Great Hall. [from Morgan et al., 2007]

to the results from 1996. The results of the two-dimensional electrical resistivity survey and their comparison with the observations from 1996 are discussed in the following chapters.

Equipment and data acquisition

The measurements of resistivity values were recorded with a resistivity meter ELREC-T produced by IRIS Instruments, France. The advantage of this resistivity meter is its capability to be used with an intelligent node system that can automatically switch the electrodes to vary source and receiver dipole positions for each measurement. All measurements were taken automatically through the control of a microprocessor and stored in the internal memory of the resistivity meter.

In 1996 all measurements were made automatically by using intelligent nodes and control of a microprocessor. In 2010, because of some technical problems, all electrodes were moved manually and the resistivity meter was controlled by an operator.

The location of the resistivity line (line B) deployed over the Great Hall is shown in Figure 8. The resistivity lines were conducted directly over the object of interest. It is known for a fact because a borehole that enters a roof of the Great Hall is located next to a road where the observations were made. The lamppost located close to the beginning of the lines was used as a benchmark and a zero location point (shown with a red star in Fig.8).

The interpretation of the resistivity data from year 1996 shows that one side of the Great Hall is located close to the position of the lamppost. Its shape can be distorted by an edge effect in the resistivity imaging [Morgan and Wharton, 1996; Shi 1998]. Therefore to eliminate the negative edge effect and obtain a better image of the Great Hall the origin of the resistivity line in 2010 was shifted by 15 meters compared to the origin of 1996 line.

The basic layout of the pseudo section array is shown in Fig.9. A pair of electrodes used to inject current into the ground is called the current dipole or current source (pictured in red color in Fig.9). The measurements of the voltage differences are made by the other pair of electrodes called the potential dipoles or receiver dipoles (shown in blue color in Fig. 9). All electrodes are placed at equal intervals along the entire length of the

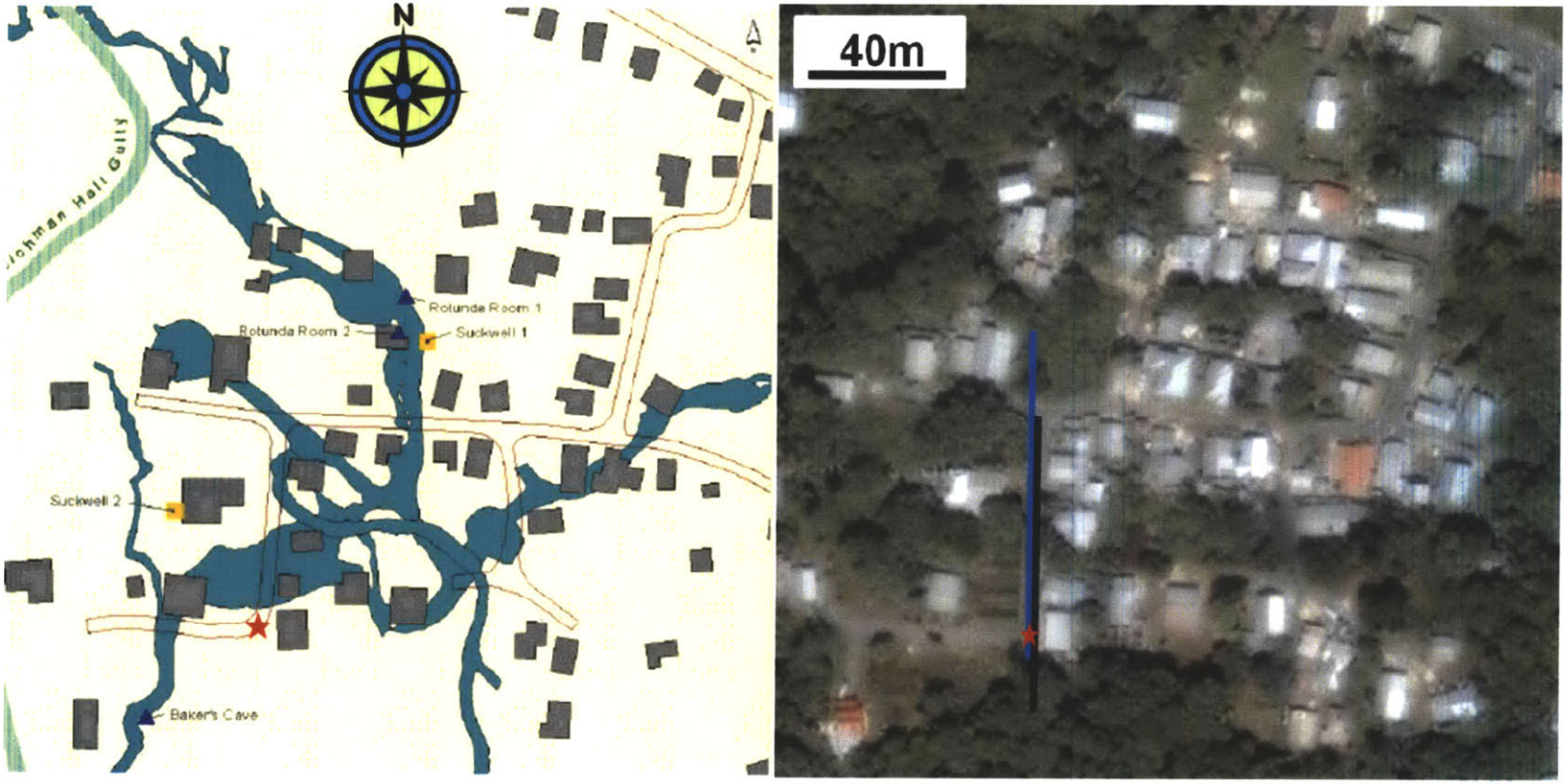

(a) (b)

Figure 8. (a) Footprint of Harrison's cave system on the street map of Allen View village (modified from fig.13 of ref. [AXIS report]); (b) location of the resistivity lines (modified from Google Maps). Line conducted in 1996 is shown in blue color; line conducted in 2010 is shown in black color. Red star represents the position of the lamppost used as a benchmark.

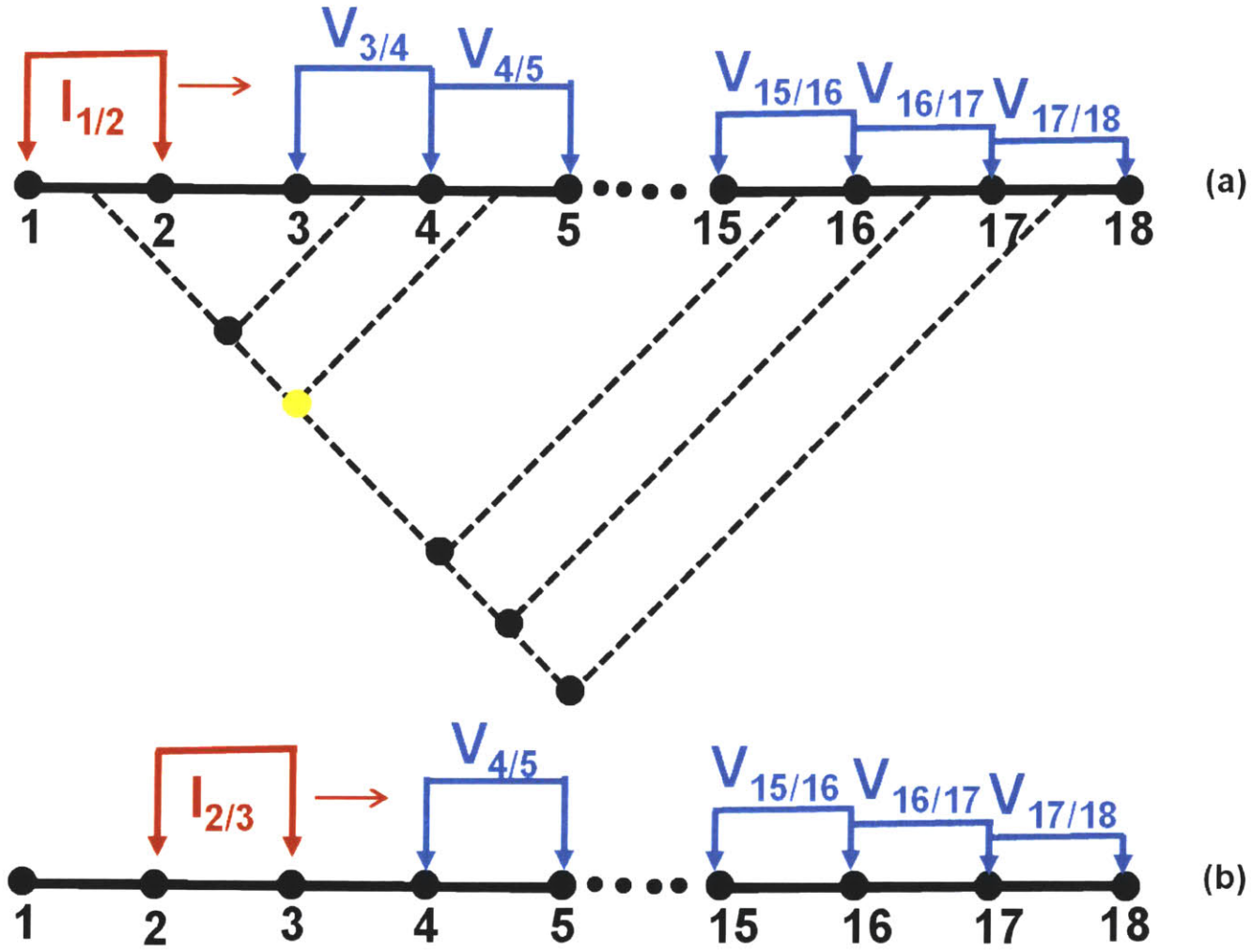

Figure 9. Layout of the pseudo section array with 18 electrodes. The current dipoles are shown in red color and the potential dipoles are represented in blue color. The horizontal red arrow shows the direction in which current sources are moved.

line. The line length and the electrode separation determine the depth of investigation and the resolution. After the current is injected by the first current dipole (electrodes #1 and #2 in Fig.9a) the potential difference is measured at all sequential receiver dipoles (ie. at the electrodes #3 and #4, #4 and #5 and so on until the end of the line, Fig 9a). When the first sequence of measurements is finished the current is injected into the next source dipole (electrode # 2 and #3 Fig 9b) and the potential differences are measured again (Fig. 9b). This process is repeated until the last current dipole is excited.

The measured potential difference is converted to the apparent resistivity values. By the convention method invented by Prof. T. Madden at MIT in 1957, the collected measurements could be related to the points in the subsurface by the rule displayed in Fig. 9a. For example, the apparent resistivity obtained from the potential difference measured across the electrodes #4 and #5 when current is injected at electrodes #1 and #2 is related to the intersection (shown as a yellow dot in Fig 9a) of the lines drawn from the middle of the current and potential dipoles at 45 degrees. The image obtained by this technique is called the pseudo-section of apparent resistivity [Madden, MIT, 1957] and gives only a rough idea about the underground structures but does not represent the true picture of the subsurface.

After collecting the data using the pseudo section electrode configuration, the left and right sweep arrays, invented by Prof. F.D. Morgan at MIT in 1996 [Morgan and Wharton, 1996], were performed. These complimentary arrays employ the spatially varying current dipole as opposed to the constant spaced source dipole in pseudo section electrode configuration. The main feature of the left and right sweep array is that one of the current electrodes is fixed at one of the ends of the line while the other current electrode gets moved.

The left and right sweep electrode configurations carried out in 1996 and 2010 were not identical. The difference in the electrode arrays between 1996 and 2010 is in the location of the receiver dipoles. In 1996, the voltage differences were measured using a reference electrode. The position of the reference electrode was fixed for all measurements where as the second electrode in the receiver pair was moved after each measurement. Therefore, the distance between the electrodes in the receiver pair varied at each measurement. In 2010, the separation between the electrodes in the receiver dipole

was kept constant and equal to 5 m. Both electrodes in the receiver pair were moved to take a new measurement point.

The conventional positions of apparent resistivity measurements collected in 2010 and 1996 are plotted in Fig.10 and Fig. 11 respectively. It can be seen from Fig.10 and Fig 11 that using pseudo section electrode configuration together with left and right sweep arrays ensures obtaining the adequate coverage of the subsurface structure. On both figures, the pseudo depths for the traditional dipole-dipole array with constant unit electrode spacing equal to 5 m are shown as greed stars whereas the pseudo depths for the configurations with varying spacing of the current dipole are pictured as small black and large red circles. The pseudo depths where two or more symbols coincide with each other correspond to reciprocal measurements.

To conclude, the summary of the technical characteristics regarding the electrode configurations used in 1996 and 2010 years are presented in this paragraph. In 1996, the 20 electrodes were deployed with 5 m separation. The first electrode was located 5 meters apart to the north from the lamppost. In 2010, 18 electrodes with 5 meter separation were used. Because the 2010 line was shifted 15 m north from the lamppost there is an overlap of 75 meters between two lines (Fig. 8).

Data quality

For each data point, the resistivity meter performs a stack with a minimum of three and a maximum of six measurements. The standard deviation for each stack is a good indicator of the quality of the data. In 2010, the relative standard deviation for each stack was checked during the measurements to ensure the good quality of the data. The quality of the 2010 data set was relatively good, with standard deviations generally below 3%. The information about the standard deviation of the data collected in 1996 is unavailable but it is known that one of the intelligent nodes was broken and some of the measurements were removed from the 1996 data set due to unacceptably high value of standard deviation (the pseudo depths for available resistivity measurements are shown in Figure 11).

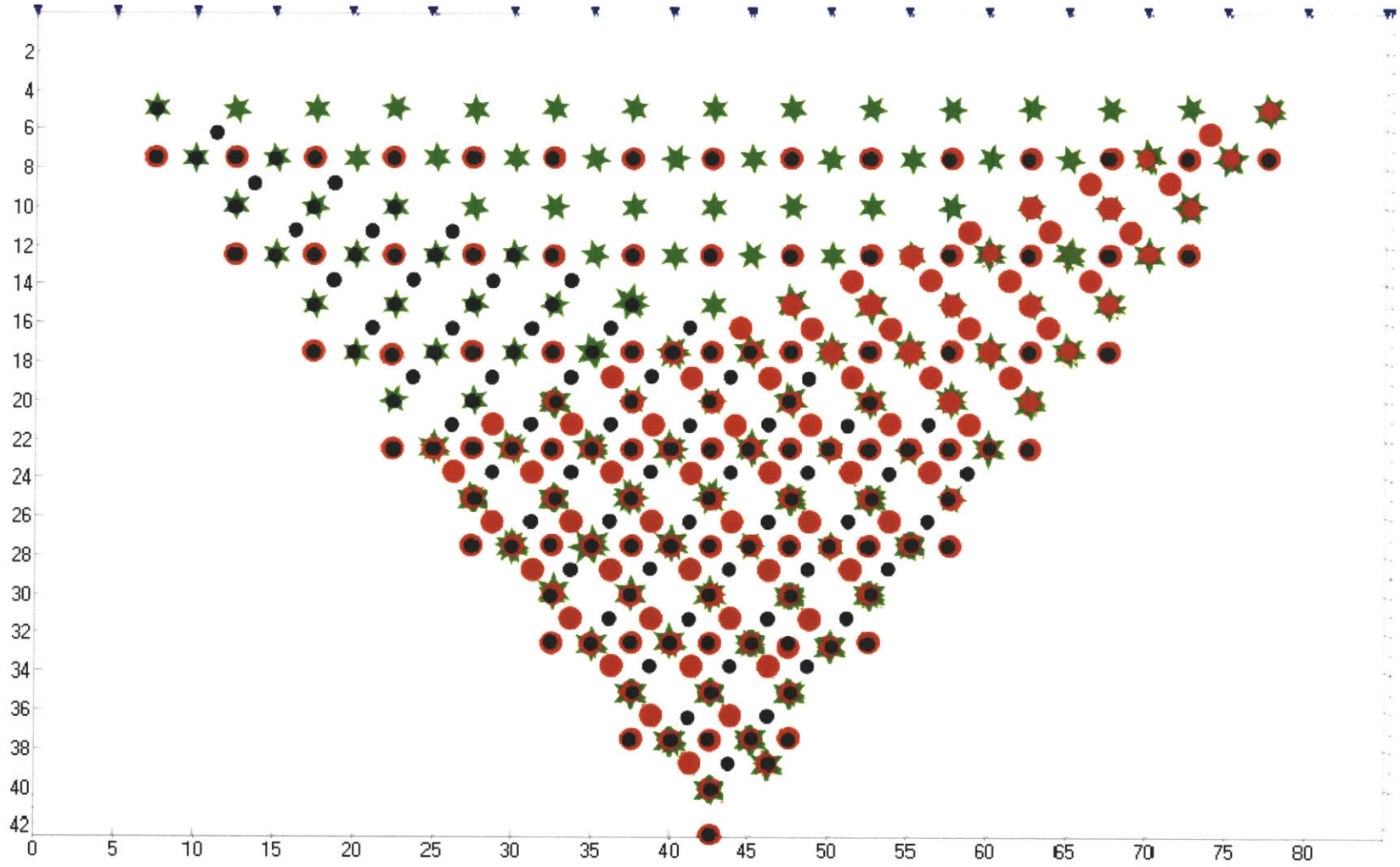

Figure 10. Pseudo depths for the traditional dipole-dipole array (green stars) and for configuration with varying spacing of the current dipole (small black and large red circles) conducted in 2010.

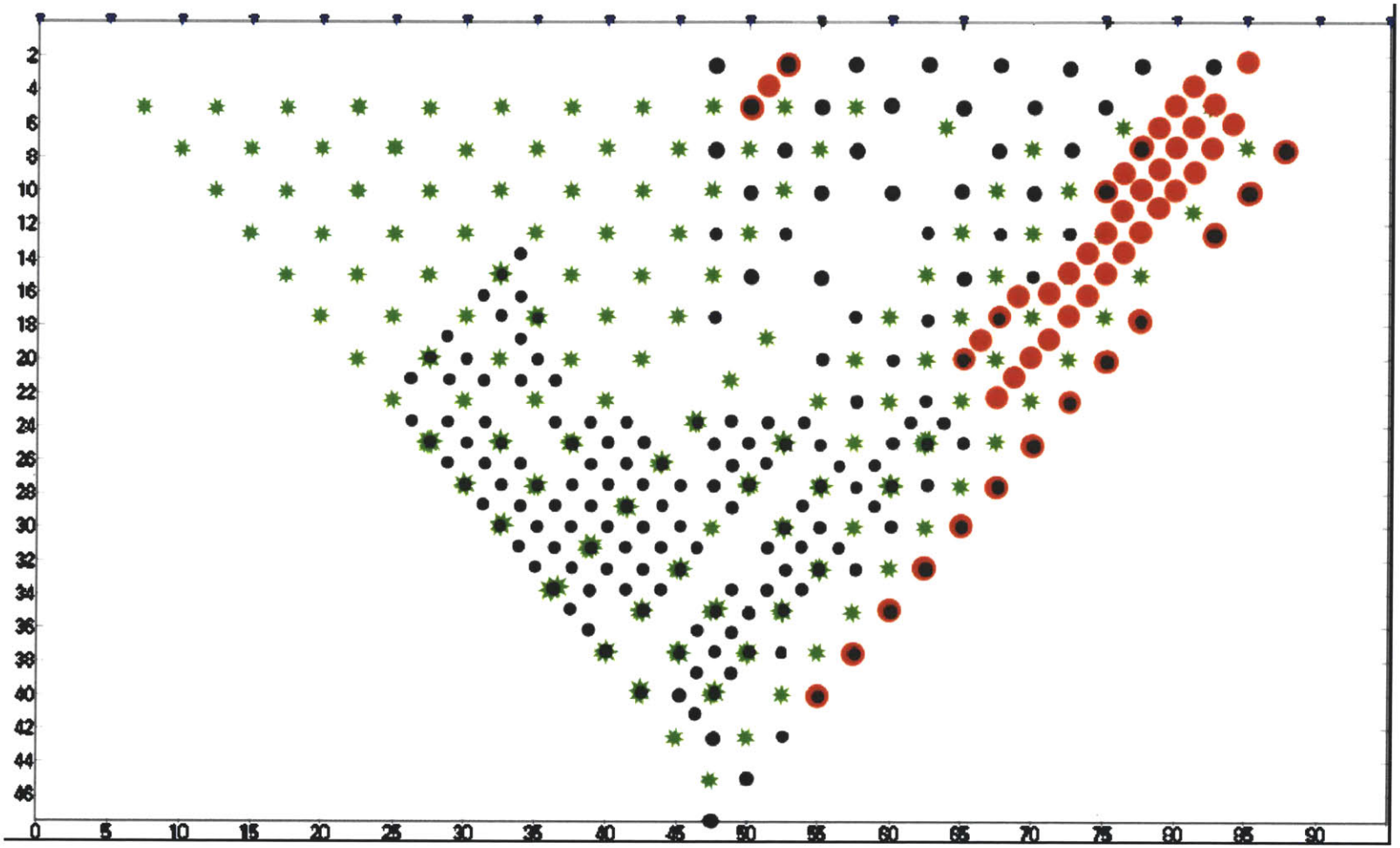

Figure 11. Pseudo depths for the traditional dipole-dipole array (green stars) and for configuration with varying spacing of the current dipole (small black and large red circles) conducted in 1996. Notice only small number of pseudo depths marked by red circles and incomplete coverage of pseudo depths marked by black circles.

Electrical Resistivity Tomography (ERT) results

To obtain the image of the subsurface, the data collected in 1996 and 2010 were inverted using a 2D electrical resistivity inversion algorithm [Shi, 1998; Zhang, 1995]. The inversion models for 1996 and 2010 data sets were defined over a 36 by 16 grid of cells and 34 by 16 grid of cells respectively.

The outputs of the inversion are presented in Figure 12. The top panel in Figure 12 shows the result of the reinterpretation of the data collected in 1996. The inversion of the recently collected data is shown in the bottom panel of Figure 12. Color scales represent the logarithm to the base ten of the resistivity values. The cave system filled with air has very high resistivity values which can be seen in Figure 12, in red color. To better establish the geometry of the cave system the approach suggested by Beard and Morgan [1991] is utilized. The idea behind this method is to qualitatively predict the geometry of an anomaly by specifying a cutoff resistivity value. All pixels with the resistivity value higher than prescribed cut off value are shaded in red (Fig. 13) showing the enhanced geometry of the caverns. The resistivity values which are less than the cut off parameter are colored in blue (Fig. 13). To obtain the enhanced image of the cave structure the cut off value of 3000 Ωm (derived from synthetic modeling) was applied to the inversion result of the data collected in 2010 (Fig.13, bottom panel). Because the resistivity tomography measurements in 2010 were taken in January during the dry season the cut off value for 2010 is not applicable to the inversion results from 1996 when the survey was conducted in August during the rainy season. To estimate the value of the cut off parameter for 1996 data the ratio between background resistivities in 2010 and 1996 was calculated and used to normalize the cut off value applied for 2010 data. The background resistivity was calculated as an average resistivity of the whole area using the geometric mean. The values of the bulk resistivity for 2010 and 1996 data sets are 315 Ωm and 125 Ωm respectively. This procedure led to the cut off value for 1996 data set equal to 1200 Ωm. The top panel of Figure 13 shows the binary image of the cave structure for the 1996 data set.

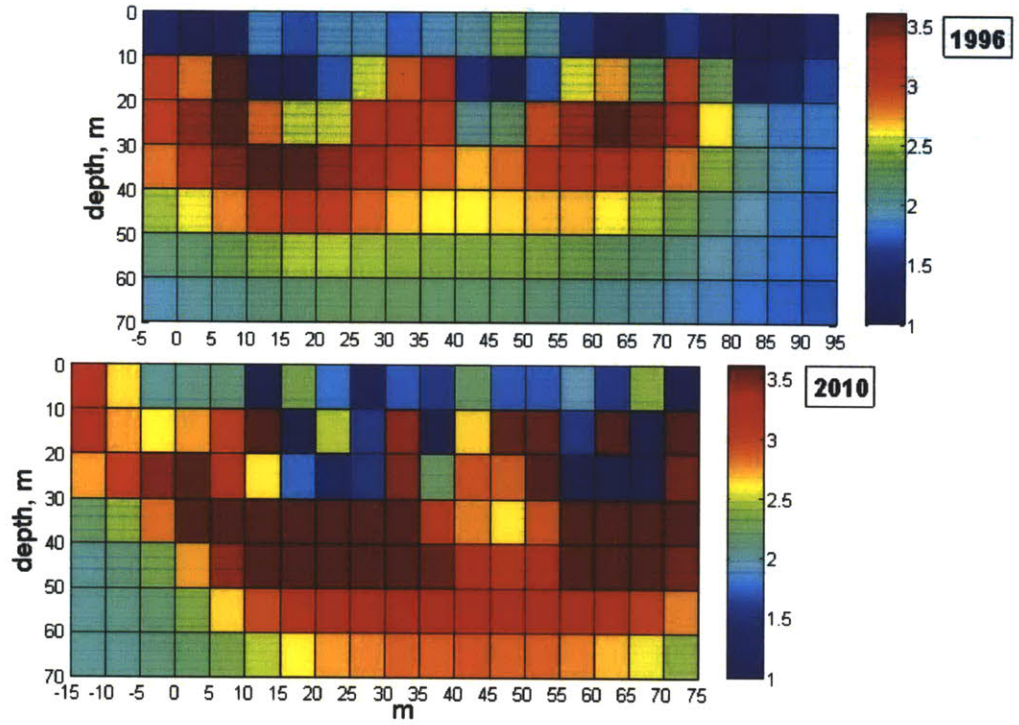

Figure 12. Results of the inversion of 1996 data set (top panel) and 2010 data set (bottom panel). The color scale shows the logarithm of the resistivity values.

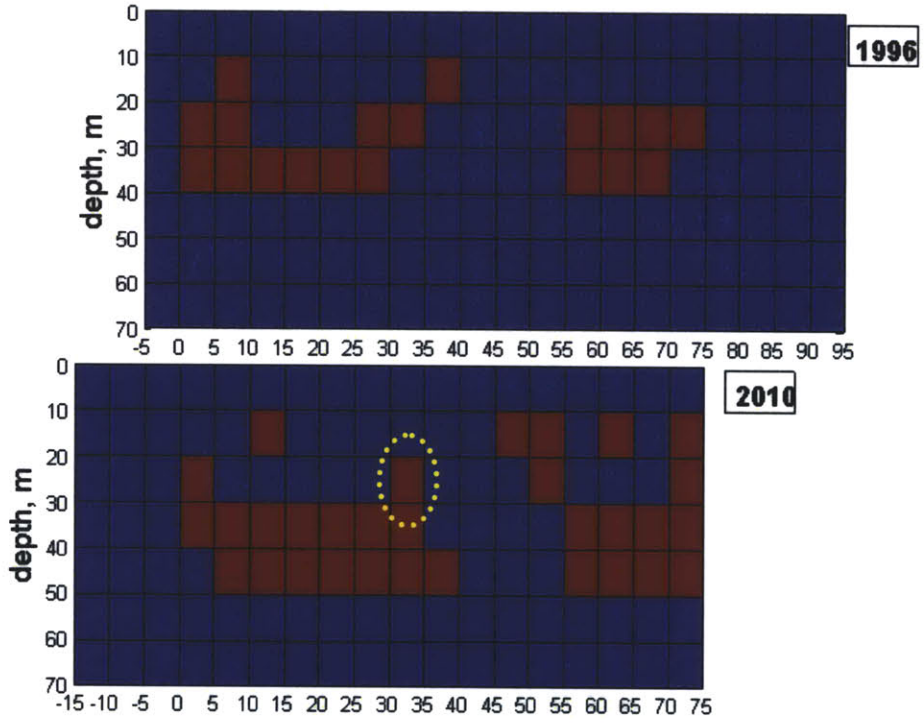

Figure 13. Binary image of the cave structure (red color) obtained by inverting 1996 data (top panel) and 2010 data (bottom panel).

Two distinct caverns are clearly seen on the inversion results from both years (Fig. 12, 13). The larger cave located close to the left boundary of the cross section is interpreted as the Great Hall. Some changes in shape of the Great Hall could be seen when the results from 1996 and 2010 are compared (Fig. 12, 13). A feature located 30 – 35 m laterally in the bottom panel of Fig. 12-13 (outlined by the dotted yellow oval in Fig.13) deserves a special attention because it could indicate a highly fractured zone which could be connected with three fractures observed on the ceiling of the Great Hall (see Fig. 6). The fact that this resistive feature begins close to the surface should cause great concern.

A smaller cavern observed in 2010 (located 55 - 75 m laterally in Fig. 12, 13, bottom panel) shows significant changes compared to the image from 1996 year (Fig. 12, 13, top panel). Three possible caverns or zones with increased degree of karstification were developed close to the roof of the second cave which could decrease the structural stability of the cave's roof.

The approach used to obtain a binary image of the cave's geometry was utilized to delineate around the existing caves the zones exposed to karstification processes. Figure 14 shows the ternary image where the existing caverns (red color) are surrounded by the highly karstified areas (orange color). The resistive feature from the bottom panel of Figure 13 (outlined by a dotted yellow oval) became more extended in Figure 14 (bottom panel) and is located only 10m apart from the surface. It can be seen from Figure 14 that two caverns most likely became connected (the connection zone is shown by the arrow).

The main difference observed between two images of the Great Hall is that the bottom of the Great Hall on the 1996 image appears to be shallower compared to the image from 2010. This is probably an artifact of the modeling. It can happen if a very resistive layer is overlaid by a conductive layer. In this situation the injected current will flow along the path of the lowest resistance close to the surface and only a small amount of current flow would reach the resistive layer. In this scenario, the conductive layer screens the underlying structures. Therefore the sensitivity of the data to the deeper resistive layer would be very small and its geometry could not be fully reconstructed. This scenario is similar to what is seen on the image of Great Hall from 1996. The first 10 meters of the

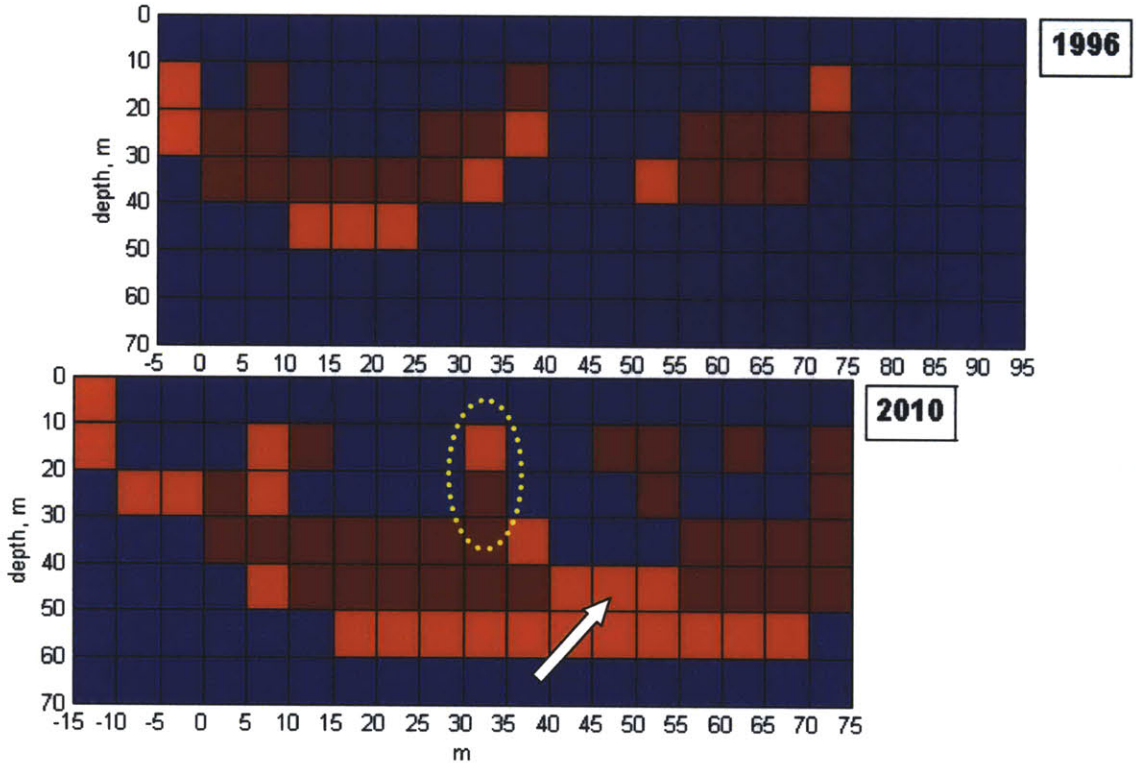

Figure 14. Ternary image of the cave structure (red color) and zones with high degree of karstification (orange color) obtained by inverting 1996 data (top panel) and 2010 data (bottom panel).

cross-section in Fig. 12(a) represent a conductive layer with the average resistivity equal to 10 Ωm which prevents the injected current from penetrating deep enough to illuminate the bottom part of the Great Hall. Therefore the vertical dimension of the Great Hall has not been reconstructed correctly from 1996 data set. The depth in 2010, where everything is more resistive, is more accurate.

Analysis of the distribution of resistivity values for 1996 and 2010 data sets can give an additional insight into the processes which happened during 14 years. Figure 15 shows the histogram of the resistivity values from 1996 (dashed black line) and 2010 (red line) data sets. It can be seen from Figure 15 that maximum of the resistivity histogram for 2010 is shifted towards the higher resistivity values. In addition, the image of the subsurface obtained from 2010 data set has more pixels with higher resistivity values than pixels from 1996 image. It suggests that in 2010 a substantially larger subsurface area is affected by karstification processes compared to 1996.

The other way to estimate to changes in the subsurface area beneath Allen View is to estimate and compare the effective porosity values for 1996 and 2010 data sets. Archie's formula (Formula 4, see page 42 for more details) defines the relationship between the resistivity of the rock matrix and pour fluid and the porosity of the rock. The pore fluid resistivity is estimated by measuring the resistivity of the water in one of the water pools inside the cave. The measured water resistivity is 25 Ωm. The values of the bulk resistivity for the 2010 and 1996 data sets are 315 Ωm and 125 Ωm respectively. Therefore, applying the Archie's law we can estimate the effective porosity. The values of the effective porosity for the 1996 and 2010 data sets are 45% and 28% correspondingly. These calculations are made under assumption that the rock matrix is saturated meaning that all the pore space is filled with water. In 1996, the resistivity survey was conducted in August during the wet season when the assumption of total saturation is valid. Whereas, the resistivity survey in 2010 was conducted during the dry season meaning that the rock matrix was drier. The important fact that for a given porosity, the measured resistivity increases as the rock becomes drier. Therefore, the decrease of the saturation value from 100% to 63% in 2010 would lead to the porosity equal to 45 %. Moreover, assuming that during the dry season the saturation decreases twofold we could get the value for the effective porosity equal to 56%.

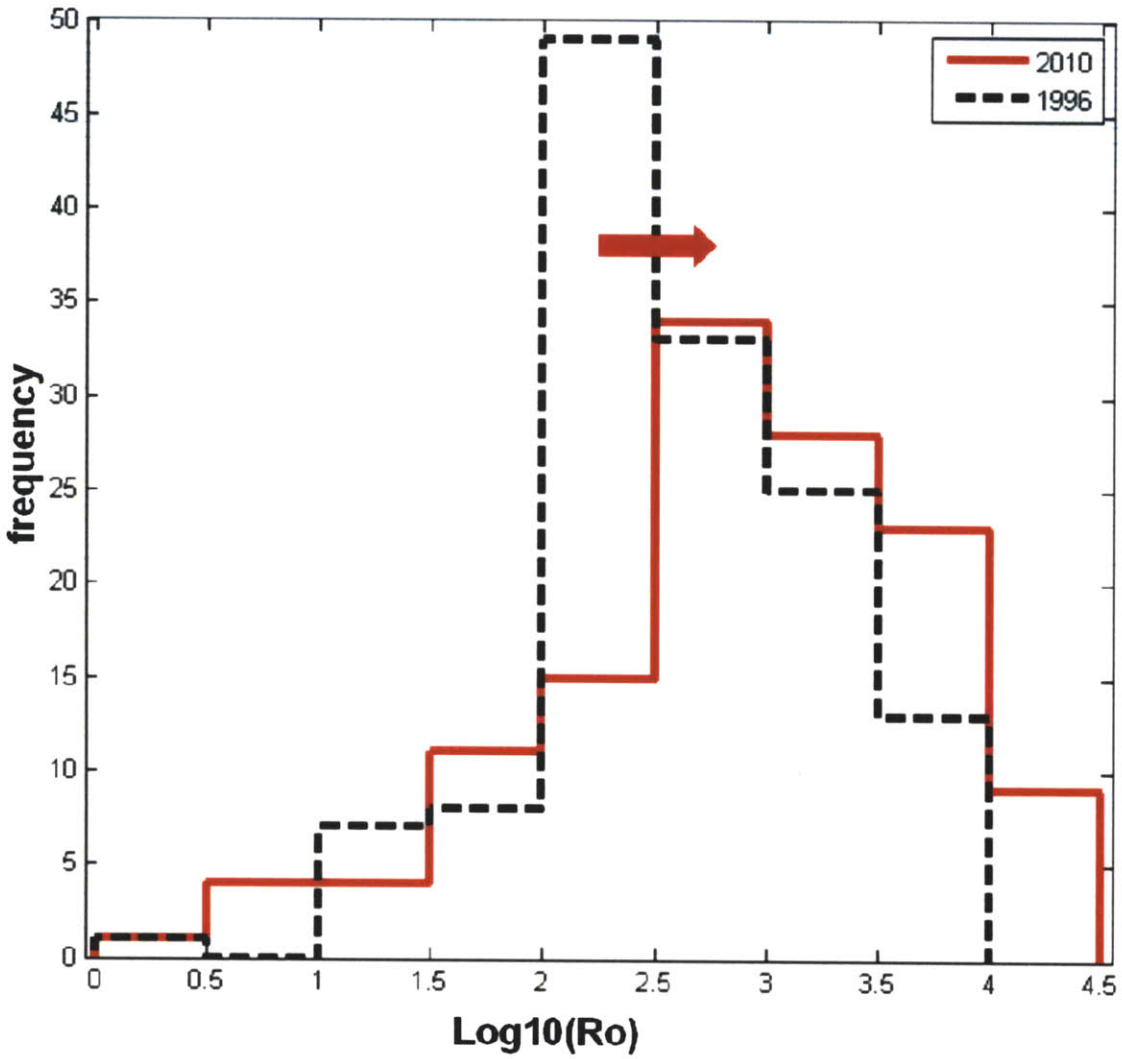

Figure 15. Distribution of inverted resistivity values obtained in 1996 (black line) and 2010 (dashed red line) data sets. Maximum of the resistivity histogram for 2010 is shifted towards the higher resistivity values (the shift is highlighted by an arrow)

Conclusion

Analysis of the results of the ERT surveys conducted with 14 years difference shows that during this time-frame significant changes happened in the subsurface roof structure of the Great Hall, Barbados. The most important observation is the increase of the karstification degree in the overburden. Not only the overburden of the Great Hall but also the overburden of neighboring cavern shows the presence of highly fractured zones that run upward from the caverns' ceiling and only a 10 m thick layer separates them from the surface. The presence of the village and the human activity would only promote and speed up the processes happening beneath Allen View. It is hard to predict an exact date when the roof will collapse. But it is clearly seen from the time – lapse resistivity inversion models that the limestone rock forming the roof of the Great Hall is highly fractured and that the fractures had progressed from 1996 to 2010. It is clear that the special actions such as a relocation of the whole village should be taken to assure safety of the village residents.

Part II: Time-Lapse ERT for Groundwater Investigation

Introduction

Electrical properties of the rocks are strongly influenced by their hydrogeological characteristics, such as the nature and amount of pore fluid, and the porosity of the fluid-bearing material. Therefore, the ERT technique could be used for groundwater investigation [Daily et al., 1992; Cassiani et al., 2006; Miller et al., 2008]. There are numerous examples in the literature that prove this potential because the ERT technique not only can discover a productive aquifer, but can also evaluate the change in water content for a certain time interval in a time-lapse mode.

The main motivation for the search for a productive groundwater aquifer in Saint Lucia is an acute demand for drinking water on the island. It is well known that the water demand in Saint Lucia is much higher than the current supply and the demand will

increase with the growth of population and further island development [Morgan 2004; Morgan, 2009; Saint Lucia natural resources project, 1986).

Fresh water in Saint Lucia is presently supplied by its extensive river system (Fig. 16). At first glance it seems that the numerous rivers could provide enough water to meet any demand of the island residents and the growing infrastructure. Unfortunately, seasonal variations in the amount of precipitation play a negative role and complicate regular water supply. In the dry season the amount of water in the rivers drops significantly. On the other hand, the rainy seasons are accompanied very often by hurricanes and landslides that lead to contamination of the river water with silt making it unsuitable for drinking. Therefore the usage of groundwater seems to be an attractive alternative to river water.

Saint Lucia is a volcanic island composed mainly of andesites with low hydraulic permeability. Geological studies of the island indicate the presence of the tuffs lenses, and also lenses composed of the products of andesite weathering such as gravel and sandstone - which can be a good aquifer. The island has a significant coverage of clays.

The current chapter shows the results of the time-lapse resistivity survey conducted during the dry and "wet" seasons to evaluate the potential and feasibility of the ground water exploration next to Thomazo River in Fond D'Or watershed in Saint Lucia. Time-lapse inversion uses resistivity data sets from two different times to determine the spatial change in resistivity which can be correlated with the change in groundwater content between the dry and wet seasons. In addition, the qualitative estimation of the clay content using the chargeability data collected by the induced polarization (IP) method is shown. Time-lapse interpretation of the ERT data sets complemented by the interpretation of the IP sounding data set reveals a lens of a porous rock that has a high potential to be a productive aquifer.

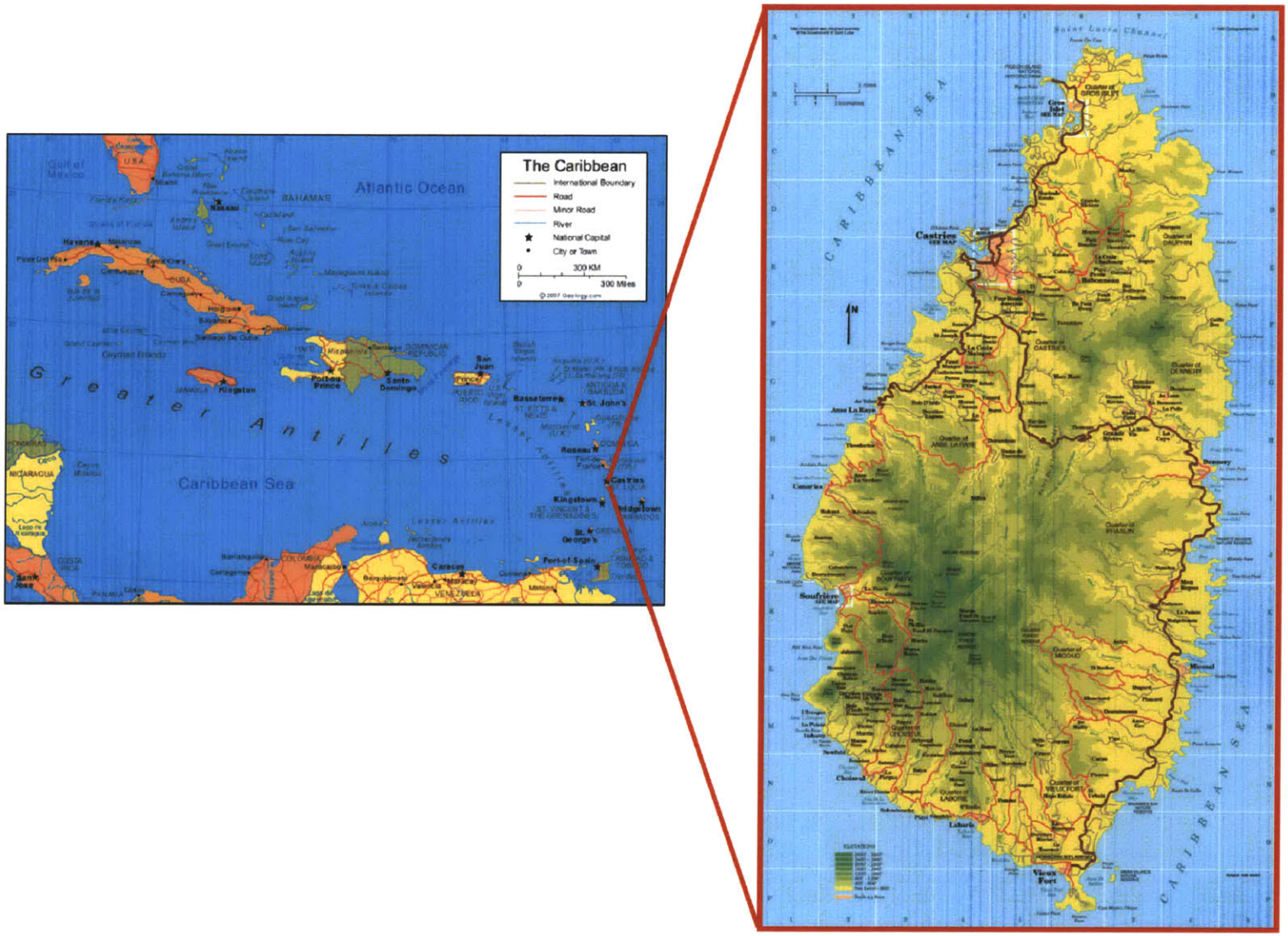

Figure 16. Geographical location of Saint Lucia.

Geology of the region

The island of Saint Lucia is located in the central part of the Lesser Antilles Volcanic Arc which emerged as a result of the subduction of the Atlantic plate under the Caribbean plate (Fig.16). The volcanic and sedimentary rocks of Saint Lucia range in age from the middle Eocene to the Holocene. The age of the rock deposits on the island decreases from north to south. Highly folded structures of Eocene basaltic rocks are predominant in the north. The subsequent weathering of the oldest basaltic rocks resulted in the formation of large alluvial plains and broad valleys in the region. During the middle Tertiary to Pliocene the central ridge and eastern coastal rocks formed volcanically as extrusive andesites, basalts, agglomerates and tuffs. The Pleistocene rocks of the southern part of the island are mainly composed of dacites and andesitic pumice. The weathering processes did not affect much of the recently formed regions of the island therefore the topography there is rugged and steep as opposed to the northern regions [Maury et al., 1990; Macdonald et al. 2000].

The study area is located in the eastern part of Saint Lucia and represents a part of the Fond d'Or watershed (Fig. 17). In the lower Fond d'Or river basin agglomerate tuffs and andesite agglomerate with mud sediments and clays represent the predominant rock types whereas andesite agglomerate, andesite ash and altered andesite are typical parent rocks in the upper part of the basin.

The topography of the island is dominated by a central mountainous ridge which runs northeast-southwest (Fig. 17). The significant areas of low relief occur only in the northern and southern ends of the island. The climate of the island is tropical with alternating rainy and dry seasons. The dry season lasts from December to May followed by the wet season during which hurricanes are common from June to November [Morgan, 2004; Morgan, 2009; Saint Lucia natural resources project, 1986).

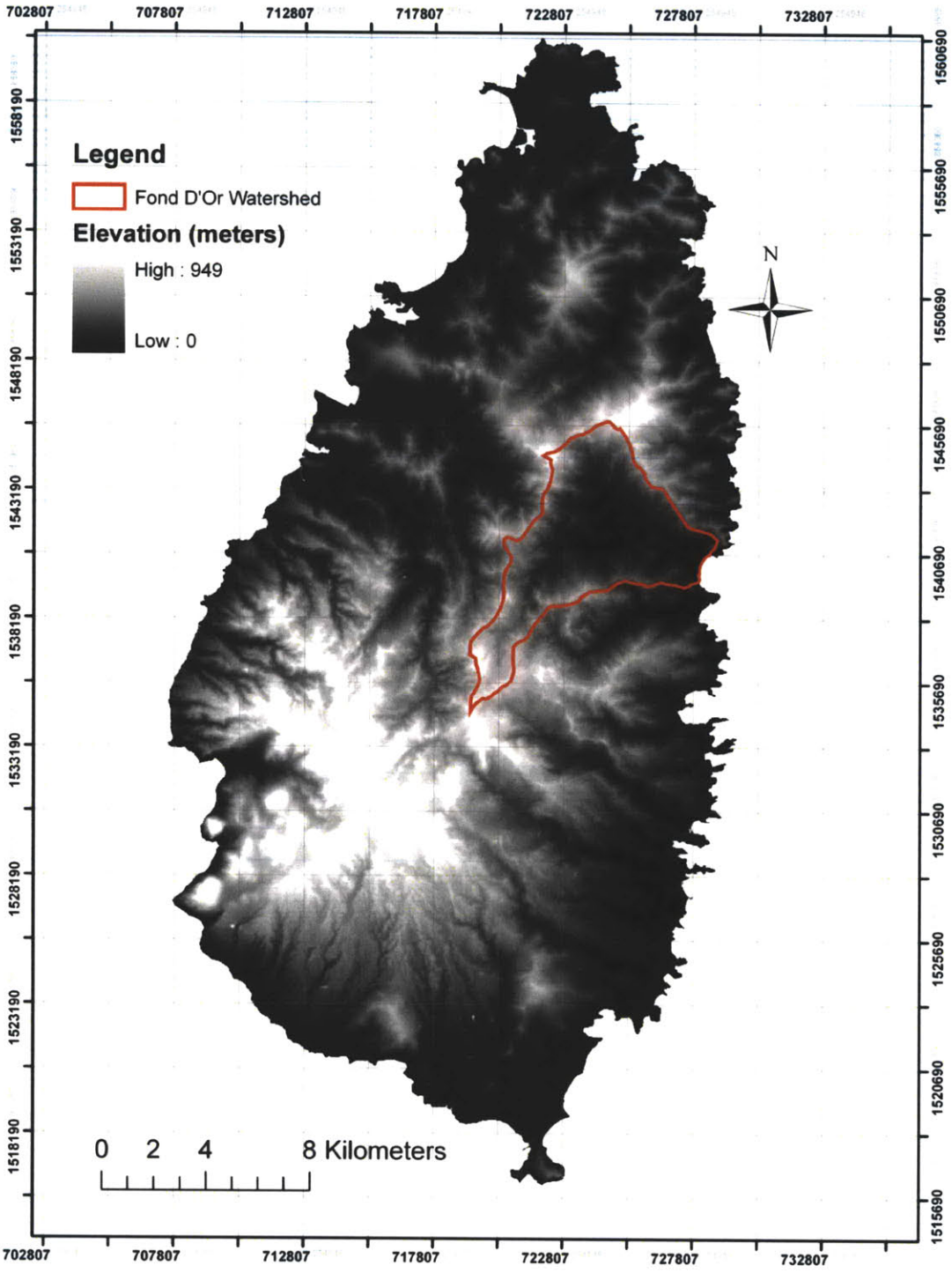

Figure 17. Topological map of Saint Lucia; the boundary of the Font d'Or watershed is outlined by orange line (modified from fig. 3.1 of ref. [Morgan, 2009])

Groundwater detection by electrical methods

Electrical properties of the rocks depend on several factors such as the nature and amount of pore fluid, and the porosity of the rock matrix. The amount of the pore fluid and its nature together with the rock matrix porosity are the most significant factors [Telford et al., 1990].

The resistivity values of common rocks, soil materials and different types of water are shown in Table 2. The resistivity of ground water varies from 1 to 100 Ωm depending on the concentration of dissolved salts. Sea water has a low resistivity (about 0.2 Ωm) due to the relatively high salt content (see Table 2).

In the absence of clay deposits in the subsurface, Archie's formula (see Formula 4) describes the relationship between the porosity and bulk resistivity of the rock and the resistivity of the fluid in the pore space of the rock [Archie, 1942]:

$$\rho_{e} = \frac{a\rho_{w}}{\varphi^{m} S_{w}^{n}} \qquad (4),$$

where ρ_e is the bulk resistivity of the rock;

ρ_w is the resistivity of water contained in porous structure;

φ is the effective porosity (ratio between the volumes of the interconnected and water filled pores with water and that of the rock);

m is the cementation factor, which indicates the size of the pores, valued between 1.3 and 2.5 (typically about 2.0) ,

a is a constant between 0.5 and 2.5, and it depends on the value of m (typically about 1 - 1.5) ,

S_w is the fraction of pores containing water, and

n is the saturation exponent (from 1.5-2.5, typically about 2.0 [Hallenburg, 1984]).

Rock type	Resistivity range (Ωm)
Distilled water	10000
Meteoric waters	30-103
Soil waters	100
Natural waters, igneous rocks	0.5-150
Natural waters, sediments	1-100
Sea water	0.2
Unconsolidated wet clay	20
Clays	1-100
Alluvium and sands	10-800
Porphyry	60-10000
Dacite	2×10^4 (wet)
Andesite	4.5×10^4 (wet) – 1.7×10^7 (dry)
Basalt	$10\text{-}1.3 \times 10^7$
Tuff	100 - 1000
Pyritic Ore	0.14-300

Table 2. Typical values of resistivity of different types of rocks, soils and water (from Telford et al., 1990)

According to this formula, the bulk resistivity of a material (estimated from ERT measurements) is a function of its porosity, saturation, and the resistivity of the pore water. We assume that the resistivity of the water in a river located near the study area can provide a good estimate of the pore water resistivity. Therefore, assuming the values for rock porosity and saturation of an aquifer and measuring the resistivity of water in a local river we can estimate the range of bulk resistivity values typical for a porous, water-bearing rock.

The measurements of the resistivity of water in Thomazo River in the Fond d'Or watershed revealed a value of 40 Ωm. Using Archie's formula (4), we estimate the range of aquifer resistivities to be 100 Ωm to 2000 Ωm with a porosity range of 15% to 60%, making the following assumptions:

1) the porosity of a typical permeable aquifer can vary from 15% to 60%
2) the water in the aquifer has the same resistivity as nearby river water (ie. 40 Ωm)
3) rocks are fully saturated (Sw = 1) with water
4) the cementation factor m varies from 1.7 to 2.2
5) the constant *a* is 1

Archie's formula as stated above assumes that the rock does not contain appreciable amounts of clay materials, as the high surface area of clays provide another conductive pathway to lower the bulk resistivity of the rock. To unambiguously determine whether the bulk resistivity of a prospective aquifer layer is defined by the presence of water in the pore space and is not affected by the occurrence of the clay it is necessary to complement the resistivity data with the measurements of IP parameters (ie. chargeability) which are sensitive to the presence of clay materials [Slater and Lesmes, 2002].

Time-lapse ERT for groundwater investigation

Pre-selection of the study area

The study area is outlined by the yellow dotted oval in Fig. 18. The Fond D'Or watershed extends for many kilometers (Fig 16, 17) and it was impossible to conduct the ERT surveys over the whole area. Therefore, a thorough pre-selection of the best site to collect the ERT measurements led us to the Thomazo River.

The following lists the main criteria for the site pre-selection [Morgan, 2009] in order of importance:

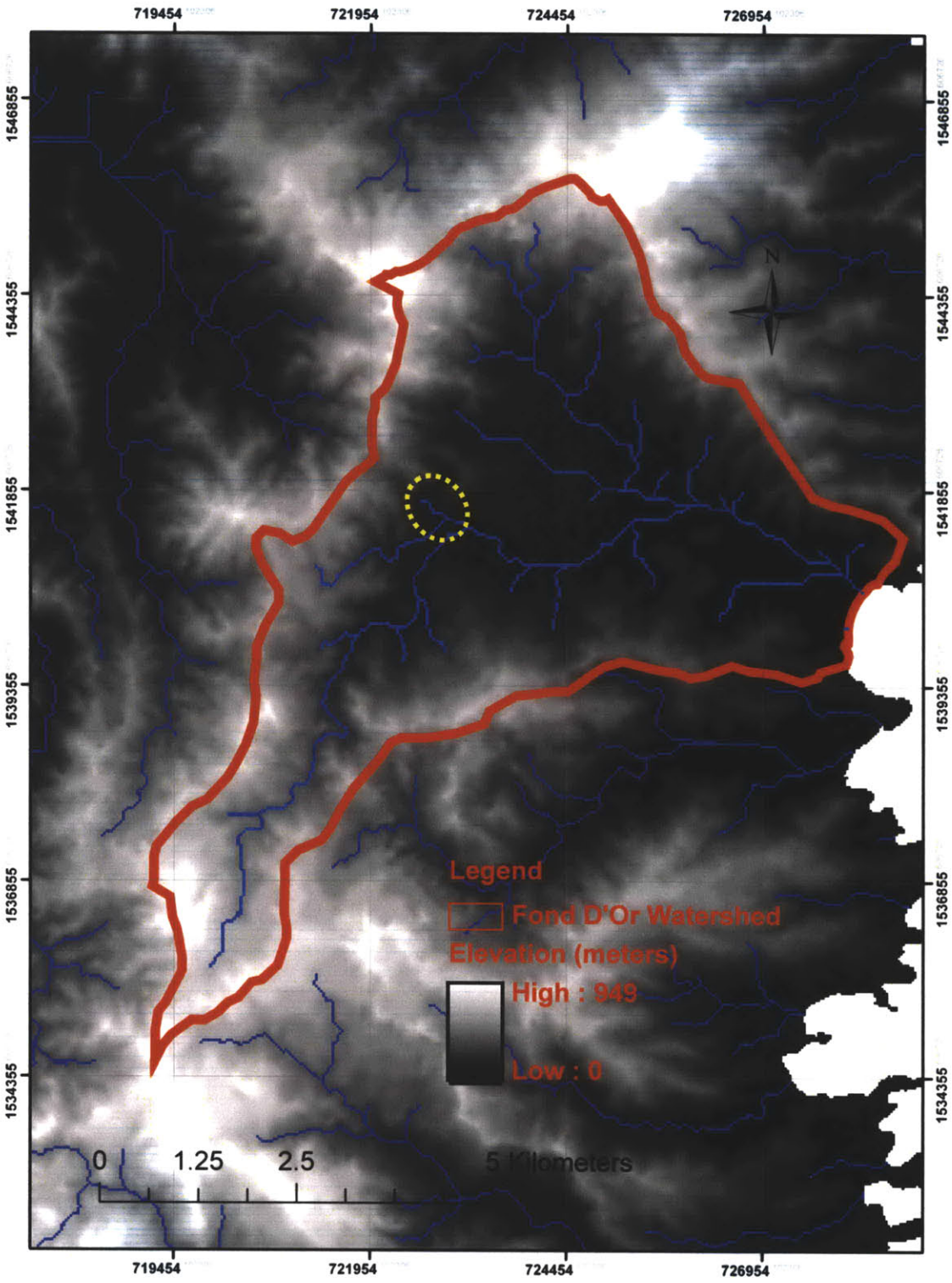

Figure 18. Topography map of the Fond D'Or watershed; Thomazo River and the study site is outlined by dotted yellow line (modified from fig. 4.1 of ref. [Morgan, 2009])

1) Easy access

Easy access (preferable by a road) to a site located in an area with mild terrain is a major requirement for drilling equipment to reach the site.

2) Proximity to a river

The aquifer discovered in an area where it will have an additional recharge from the river water. Also, the rivers tend to form in the lowest elevation in a region. It is beneficial for an aquifer to be located close to a river because the regional groundwater flows towards lower elevation providing an additional source of recharge which is relatively insensitive to seasonal variations.

3) Site elevation and topology

Only relatively flat areas of intermediate elevation were considered because they provide an adequate groundwater recharge and the thick soil layer acts as a natural filter promoting high quality groundwater.

4) Geology of the region

Most of the bedrock in the Fond D'Or valley is andesite overlaid by clays, with occasional layers of tuff. The sites where the bedrock is exposed or near to the surface were ignored. On the other hand, the areas where the highly porous tuffs and the products of early weathering of the andesites (sand and gravel) are present are promising for further investigation.

Filed data acquisition

Acquisition of the electrical resistivity tomography data

The first set of resistivity data was collected at the end of March during a dry season. The preliminary interpretation of this data set indicated the existence of a possible aquifer just beneath the Thomazo River, but for more accurate estimation the investigations of the same site during a rainy season is required. Therefore, it was planned to repeat the resistivity measurements during the rainy season; this was done in

the middle of December in 2010. Usually, a dry season starts in December but in 2010 an anomalous climate situation was present in Saint Lucia which brought a severe hurricane in the beginning of November followed by the heavy rains. The heavy rains in November had caused flooding of the low relief areas and numerous landslides in the topographically elevated areas. The enormous amount of precipitation in November suggests that the wet season finished later than usual. For that reason we assume that the ERT data collected in December characterizes the wet season conditions.

The location of the resistivity line is shown in Figure 19 where the beginning of the line is indicated by a green circle. The total length of the line is 100 m. The resistivity line crosses the Thomazo River between 45 and 50 m from the origin of the line.

The data were collected using the standard dipole – dipole configuration (for the description of the method see page 24) with constant spacing of the source and current dipoles. In order to obtain a good resolution at shallow depth, the unit electrode spacing was chosen to be equal to 5 m. To achieve larger depth of investigation the unit electrode spacing was increased to 10 m. The electrode configuration and conventional positions of apparent resistivity measurements (see page 24 for more details) are shown in Fig. 20 where the electrode positions are marked by the triangles at the top of the pseudosection. The conventional positions of apparent resistivity measurements collected with 5 m unit electrode spacing and 10 m unit electrode spacing are shown by blue crosses and circles respectively. As an example, the measurement of apparent resistivity where the current and potential dipoles were located at the positions denoted as AB and MN correspondingly relates to the subsurface area shown by a square.

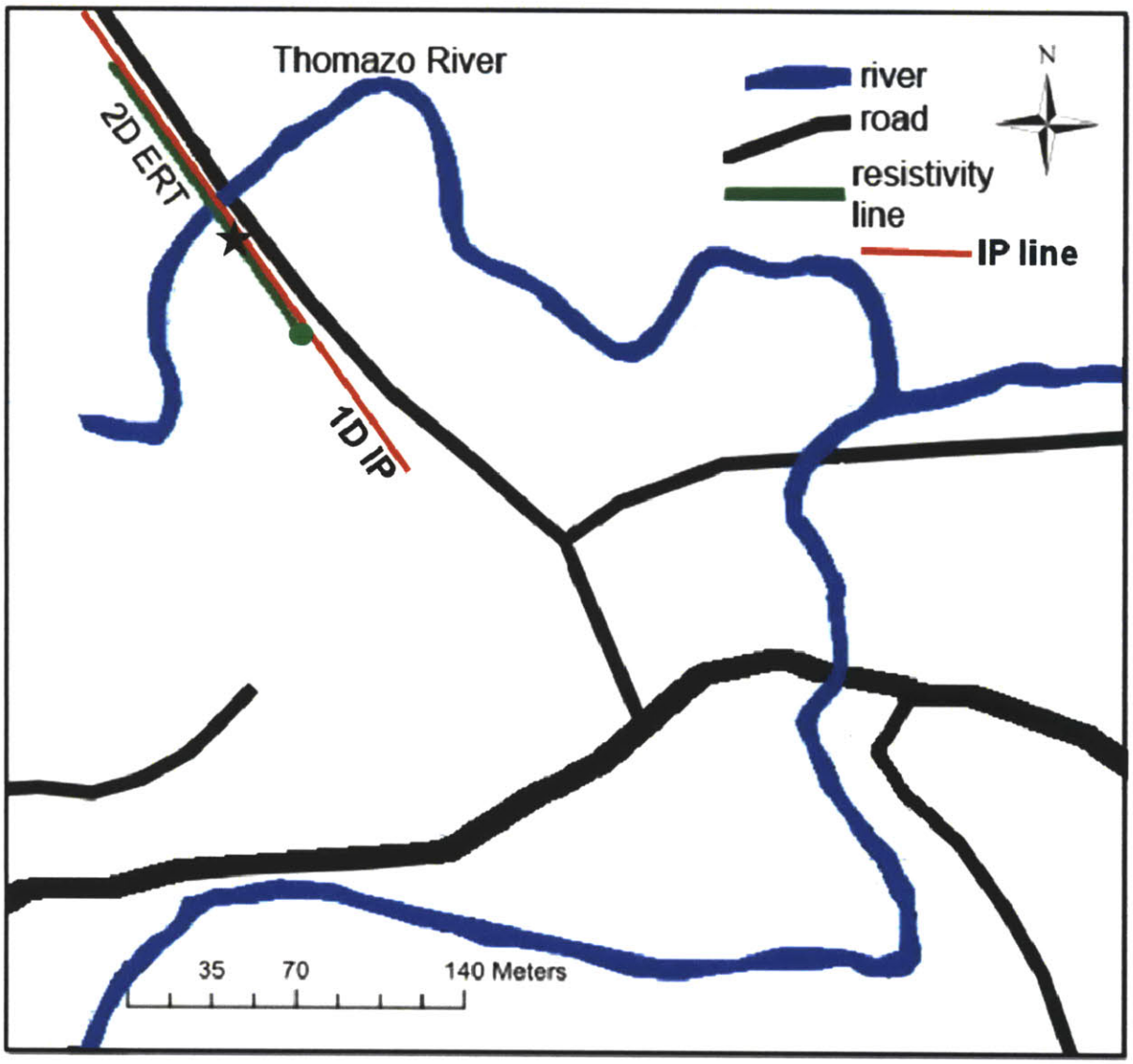

Figure 19. Close-up of the study area at Thomazo River, Fond D'Or watershed (modified from fig. 4.4 of the ref. [Morgan, 2009]). Location of the ERT survey line is shown by green line; location of 1D IP survey line is shown by red line. Green circles shows the beginning of the ERT line and black star shows the center of the IP line.

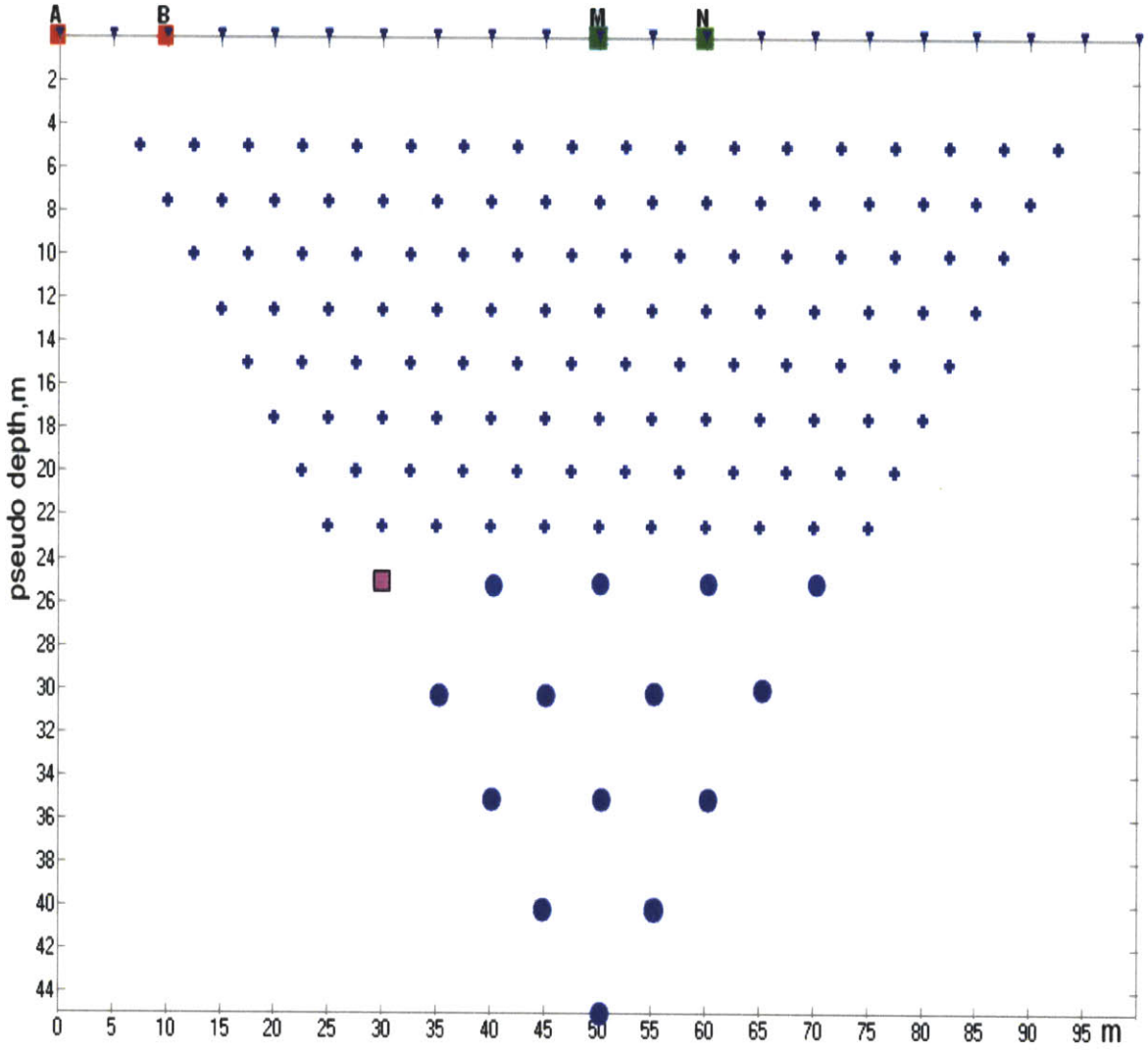

Figure 20. Dipole-dipole configuration and conventional positions of apparent resistivity measurements. Blue crosses represent the measurements collected with 5 m unit electrode spacing; blue circles represent the measurements collected with10 m unit electrode spacing. Pink square represents the conventional position of apparent resistivity obtained by current injections in the electrodes marked as A and B and the voltage difference measurement at the electrodes marked as M and N

Acquisition of the IP data

The one dimensional induced polarization (IP) sounding survey was conducted in January 2011 to detect the occurrence of clay layers at the Thomazo River site. The location of the survey line is shown in Fig. 19 by a red line. The maximum separation of the outer current electrodes is 200 m.

A four electrode array called the Schlumberger array was employed to obtain the IP data (Fig. 21). Two outer electrodes (marked as A and B in Fig. 21) are used to inject a current into the ground. A voltage difference is measured between two inner electrodes (labeled as M and N in Fig. 21). All electrodes are positioned symmetrically with respect to the center of the line. After each measurement, the separation between the current electrodes is increased by moving the outer electrodes outward while the potential electrodes remain fixed. Increasing the spacing between electrodes A and B allows the current to penetrate a greater depth. The maximum depth of the investigation is constrained by the maximum separation between current electrodes.

The distance between the potential electrodes M and N is chosen to be five to ten times less that the distance between the current electrodes. When the ratio of outer-to-inner electrode spacing becomes more than 10, the potential electrodes are moved outward to keep the ratio AB/MN less than 10 in order to provide a good signal-to-noise ratio. For the small separations between the current electrodes A and B, relatively dense sampling is required to ensure appropriate depth sensitivity. For large electrode separations the density of sampling should be decreased because the resolution of the measured data decreases with depth. Therefore, the current electrode spacing is defined on the logarithmic scale. Usually 10 points per decade of the outer electrode spacing are enough to provide appropriate depth sensitivity.

The current injection into the ground triggers the polarization of the subsurface material. After the current shutoff, the induced polarization effect is observed as a voltage decay curve. The IP response in the time domain is called the chargeability M and defined by the following formula [Ward, 1990]:

$$M = \frac{\int_{t_s}^{t_f} V_s dt}{V_{MN} \Delta t} \qquad (5)$$

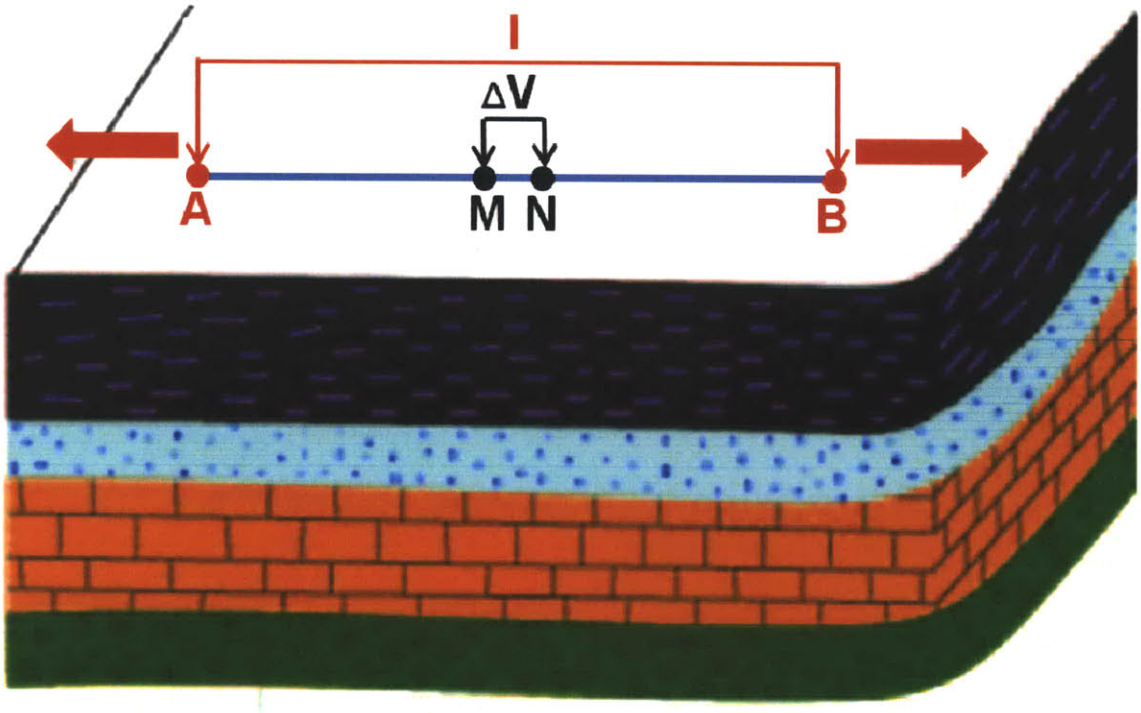

Figure 21. Schematic of Schlumberger array used to perform 1D IP sounding. The current electrodes are marked by A and B; the potential electrodes are marked by M and N

where V_s is a residual voltage integrated over a time window defined between times t_s and t_f after termination of an applied current;

V_{MN} is the voltage difference measured between electrodes M and N during the current injection;

Δt is the length of the integrated time window.

M is chargeability typically expressed as millivolts per volt (mV/V).

In addition to the chargeability measurements, the resistivity data was collected as an aid to normalize the chargeability data.

Interpretation of the field measurements

Time – lapse inversion of the ERT data sets

Figure 22 shows the pseudo-sections of the apparent resistivities measured during dry (top panel) and "wet" seasons (bottom panel). Because the apparent resistivity values are not equal to the true values of the resistivity in the subsurface, the inversion was conducted to obtain the true resistivity values of the subsurface rocks.

The inversion models were defined over a 37 by 25 grid of rectangular cells with the dimensions 5 by 2.5 m.

The results of the inversion of each data set revealed a lens body of varying resistivity beneath the river from a depth of about 10 m, presumably overlaid by a clay layer (Fig. 23). As it was expected, the average resistivity of the lens decreased in the wet season. This result agrees well with the prediction for the wet season when a larger amount of water is present in the lens.

Based on the inversion results the average resistivity (calculated as geometric mean) of the rock composing the potential aquifer is estimated as 150 Ωm during the dry season and as 115 Ωm during the "wet" season.

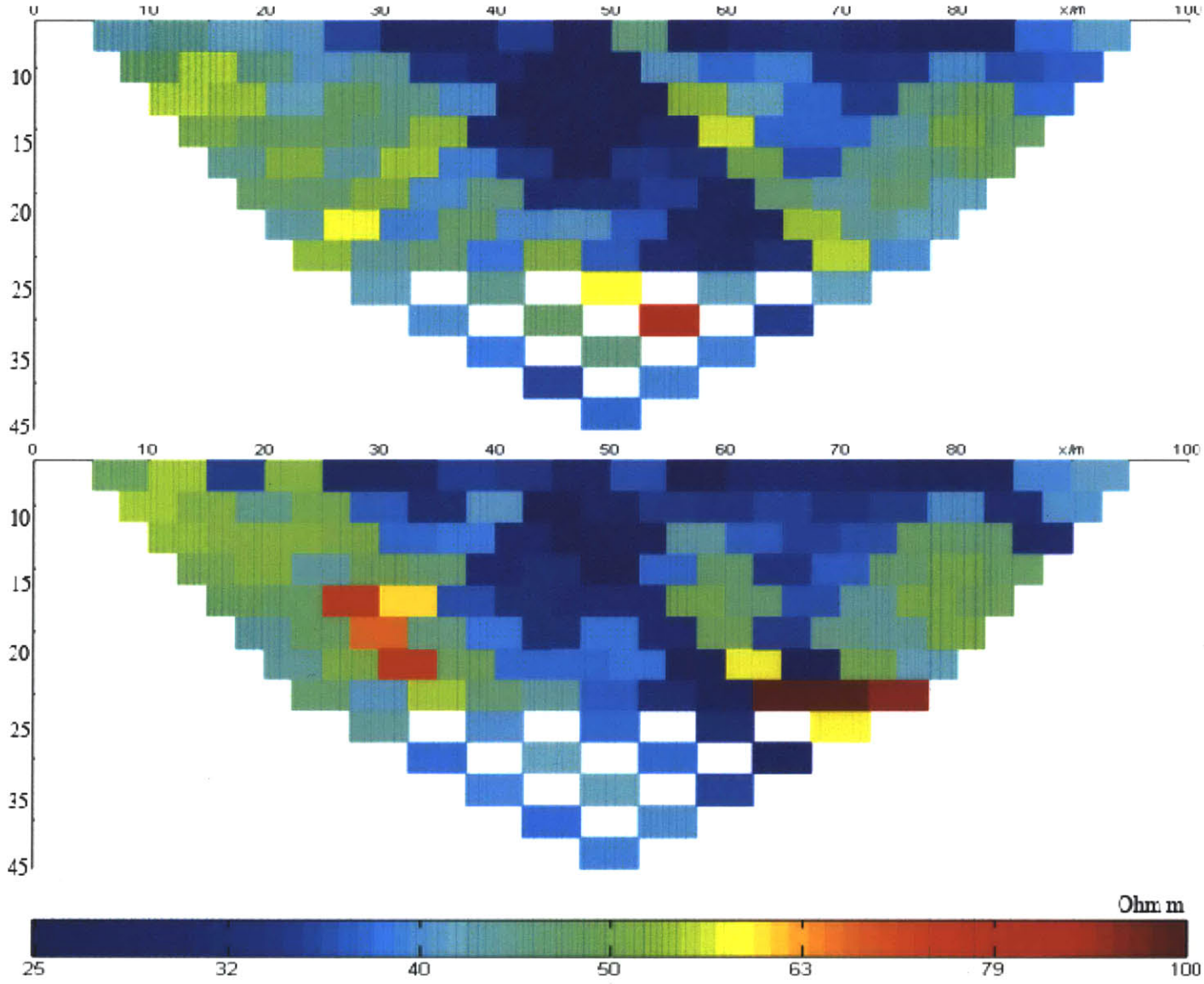

Figure 22. Pseudo section of apparent resistivities measured during dry season (top panel) and wet season (bottom panel)

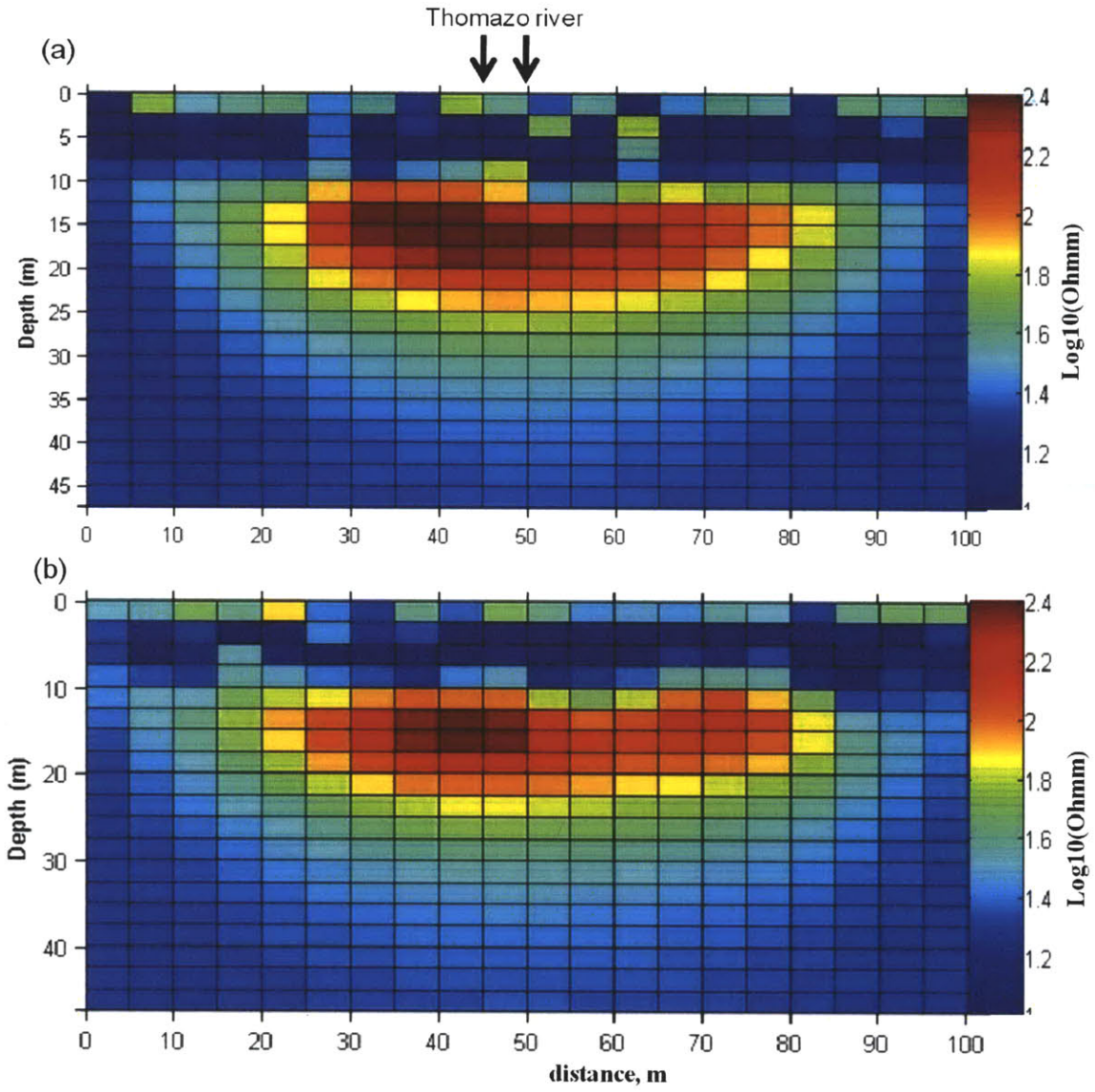

Figure 23. Results of the inversions for (a) data set collected during dry season, (b) data set collected during wet season

The analysis of the resistivity distribution can provide useful information about overall changes of resistivities between dry and wet seasons. Figure 24 shows the histogram of the resistivity values corresponding to the layer where the lens of interest is located (between 10 and 25m vertically in Fig. 23). It can be seen from Fig. 24 that for the data collected during the dry season, the inversion image has larger area with resistivity values higher than 150 Ωm (see dashed black line in Fig. 24) compared to the inversion result of data obtained during "wet season". The characteristic feature of the resistivity distribution of the "wet" season (red line in Fig. 24) is that the pixels with resistivity values ranging from 65 to 150 Ωm noticeably exceed in number those of the dry season inversion image. The pixels of the "wet" and dry seasons' data inversion images with resistivity values below 65 have almost identical distributions.

The distribution of resistivity values corresponding to the subsurface layer of depth between 10 and 25 m (where the lens is located) reflects the overall decrease of resistivity of the aquifer during the "wet" season. It might imply that in March 2010 (during the dry season) the aquifer contained less water than in December 2010 during the "wet" season.

To estimate the changes in the resistivity values between different seasons, we looked at the ratio of the inverted resistivity values rather than their difference. The ratio of resistivity values between dry and "wet" seasons was calculated by the division of the resistivity values pixel-by-pixel from two inversion models. The obtained ratio relates to the ratio of the porosity and saturation values by Archie's law (Formula 4). Consequently, the ratio of the bulk resistivities in wet and dry season could give an estimation of the effective porosity change:

$$\frac{\rho_{dry}}{\rho_{wet}} = \frac{\varphi_{wet}^2}{\varphi_{dry}^2} \qquad (6)$$

The time-lapse analysis was conducted to calculate the ratio of electrical resistivities which are related to the changes in water content and porosity (formula 6). The square root of the time-lapse inversion results was taken to estimate the porosity changes. Figure 25 shows that the change in the effective porosity between the dry and rainy seasons is about 15%. The regions of the lens body where the changes in water content are higher than 15% are outlined by a pink line (Fig. 25b).

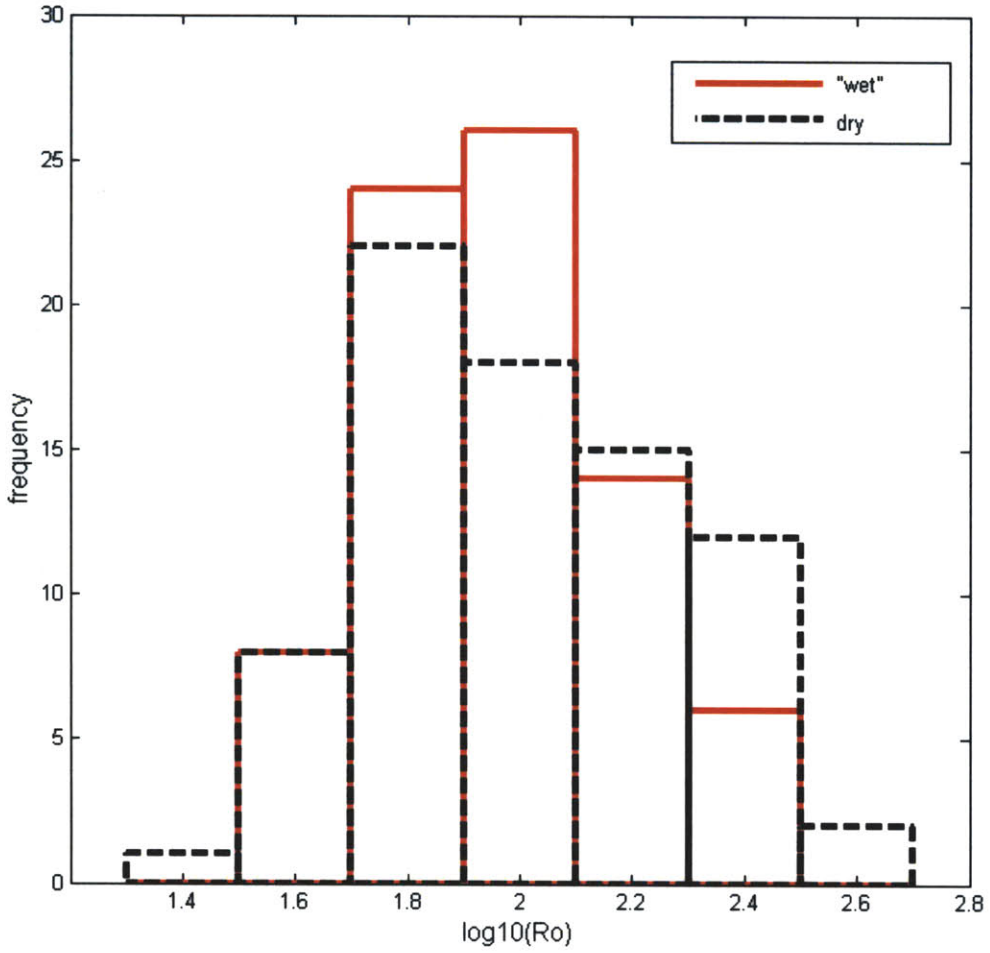

Figure 24. Distribution of the resistivity values obtained inverting the data set collected during dry (dashed black line) and wet (red line) seasons

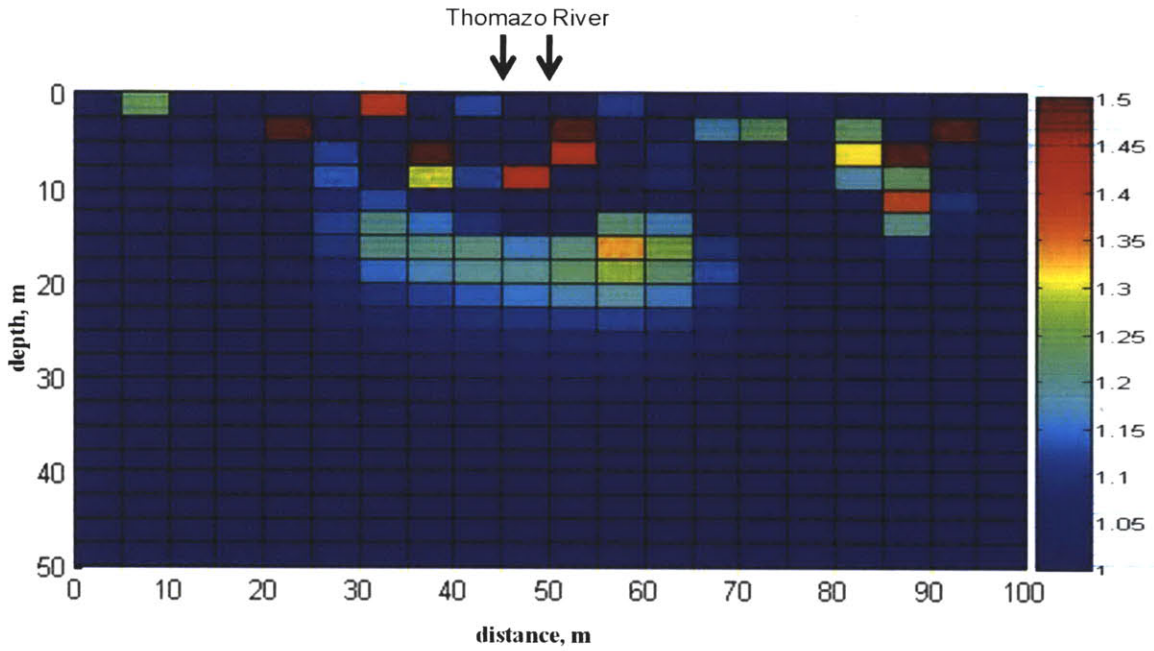

(a)

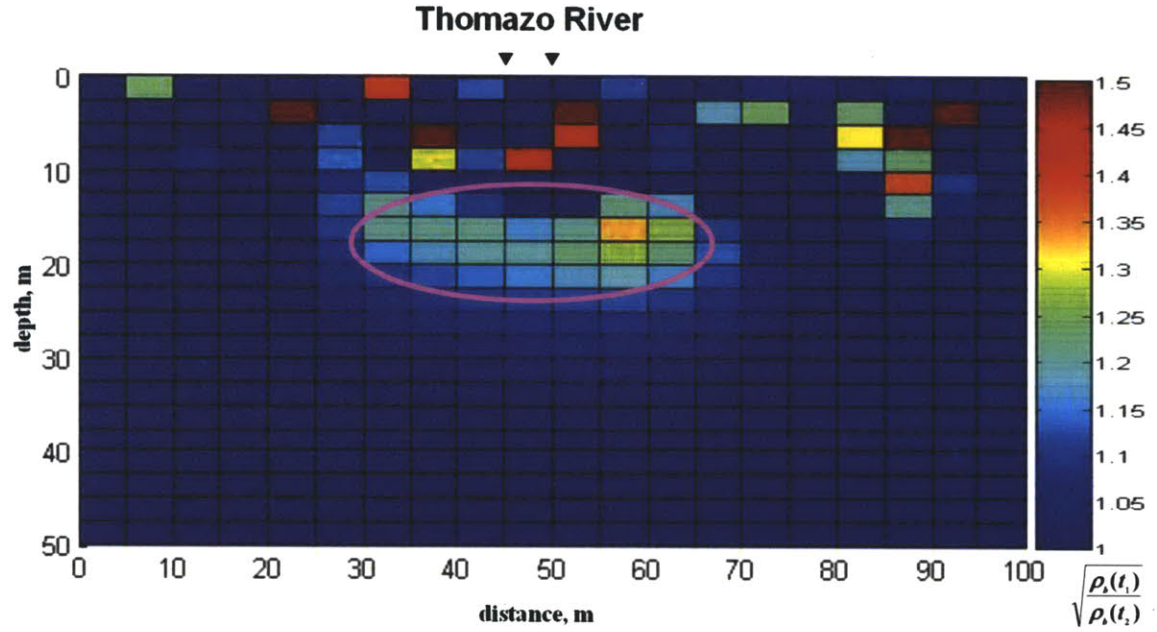

(b)

Figure 25. Output of the time-lapse inversion showing the change in effective porosity between dry and wet seasons. The pixels equal to unity show no changes. The regions of the lens body with 15% change of water contend are outlined by a pink line (b)

Interpretation of the IP measurements

Laboratory and field experiments aiming to determine the dependence of the standard and normalized IP parameters on the clay content [Lesmes and Frye 2001; Slater and Lesmes, 2002] have shown that the chargeability normalized by the resistivity value is directly related to the clay content. Therefore, we use normalized chargeability values to determine if the potential aquifer detected by the ERT survey is contaminated with clay minerals.

The 1D resistivity profile (Fig. 26a) shows that at depth between 10 and 20 m there is a resistive layer (about 125 Ωm). The resistivity of this layer and its location at depth is in a good agreement with the average resistivity of the lens (about 150 Ωm) during the dry season and the lens location vertically.

The values of normalized chargeability (Fig 26b) for the layer at a depth between 10 and 20 m are small (about 0.03 mS/m) suggesting that little or no clay minerals are present in the prospective aquifer.

The apparent resistivity curve has a S-shaped twist (outlined by the black dotted oval in Fig.27a) which was not resolved with the modeling. The appearance of this S-shaped twist is most likely due to the presence of lateral inhomogeneity. This lateral inhomogeneity is the left side of the lens discovered by the ERT survey. The center of the 1D sounding line (indicated by the black star in Fig. 19) coincides with 35m mark on the horizontal axes of the 2D resistivity image. It is clearly seen in Fig. 23 that the left side of the lens is positioned at 30 m. Therefore, the one-dimensional approximation is not accurate and the 1D resistivity data set is affected by the presence of a two- dimensional anomaly. The apparent chargeability curve is mostly smooth (Fig.27b) showing no distinguishable effect of the lateral inhomogeneity on the shape of the apparent chargeability curve. Fits for both the apparent resistivity and apparent chargeability are good enough to give confidence about the inversion results.

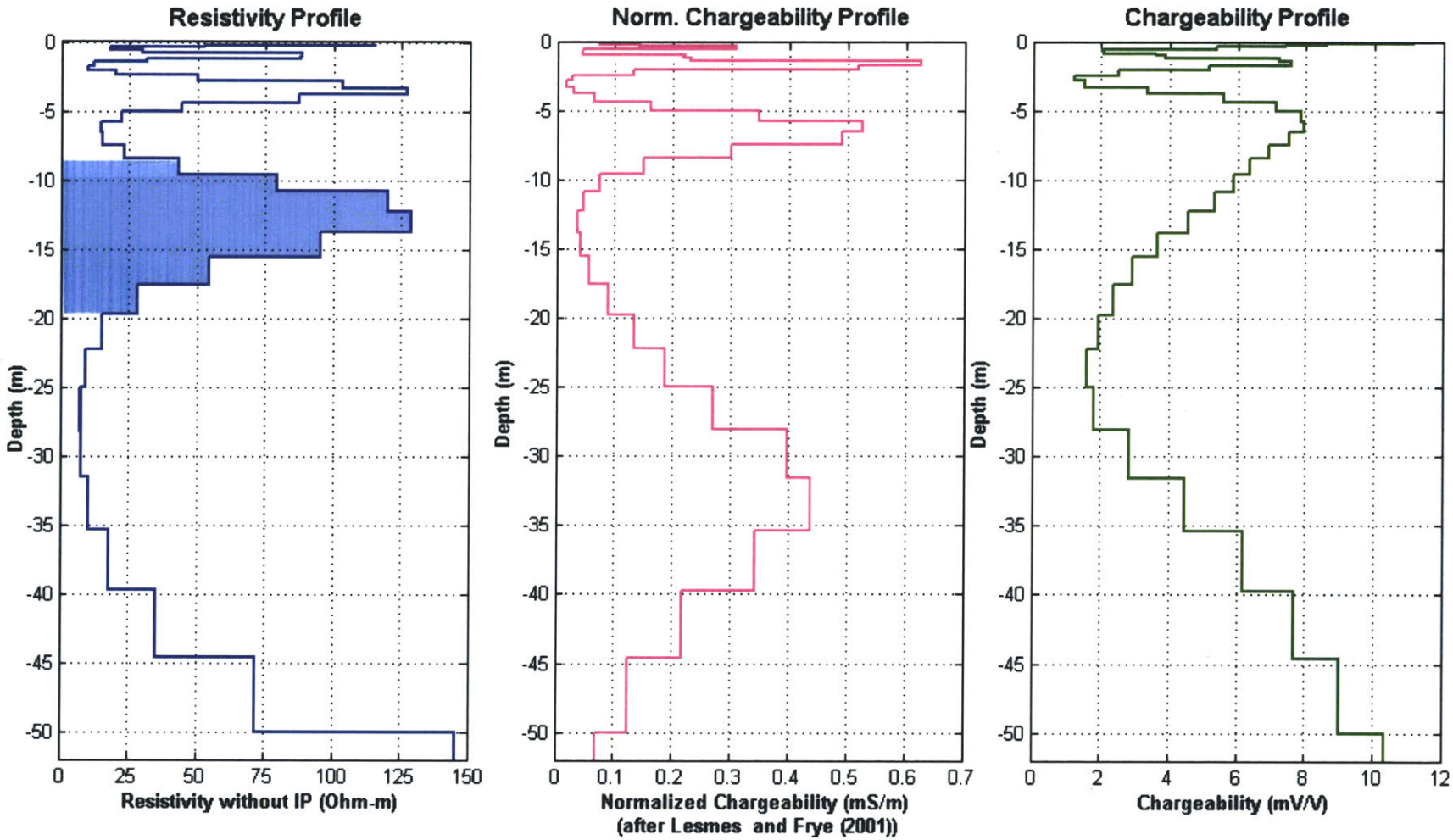

Figure 26. Resistivity (a), normalized chargeability (b), and chargeability (c) profiles at the Thomazo River site. The potential aquifer is highlighted by blue color on the resistivity profile (a)

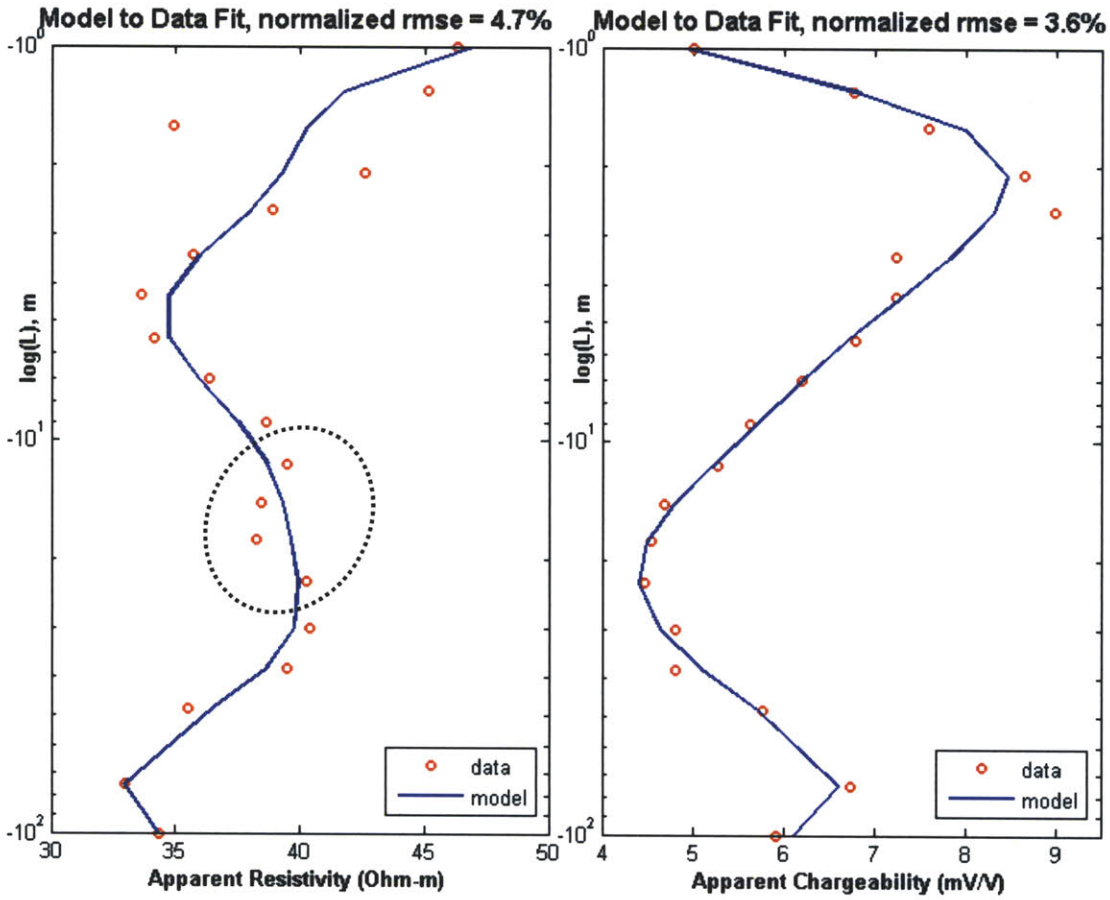

Figure 27. Model to data fits for apparent resistivity (a), and apparent chargeability (b). Black dotted oval outlines the S-shaped twist in the apparent resistivity curve resulted from the presence of lathers inhomogeneity

Preliminary estimation of the water content in the aquifer

The measurement of the water conductivity in Thomazo River was of value 25 mS/m which is equivalent to a resistivity of 40 Ωm. Based on the inversion results the average resistivity (calculated as geometric mean) of the rock composing the potential aquifer is estimated as 150 Ωm during the dry season and as 115 Ωm during the "wet" season.

The result of the inversion of the IP data indicates that the lens is not contaminated with clay; therefore Archie's formula can be applied to calculate the effective porosity of the prospective aquifer. The evaluation of the porosity with Archie's law setting water resistivity equal to 40 Ωm and bulk rock resistivity to 105 Ωm, assuming the total saturation during the "wet" season and the cementation factor equal to 2 reveals a porosity of 59%. The high value of the porosity of the rock suggests that the aquifer is most likely composed of pumice whose porosity can be as high as 85%.

Based on the results of the ERT survey, the thickness of the lens is estimated as 10 m whereas its length is at least 35 m. We assume that the lens has the same length and width equal to 35 m. Therefore, the approximate volume of the potential aquifer is estimated as 12250 m^3 which is equivalent to 12.25×10^6 liters. The next step is to assume how much water can be pumped from the underground. In general, only about 40 % of the groundwater can be extracted from an aquifer. The Archie's law estimate for the porosity of the rock is 59%. By multiplication (Formula 7) of all components defined above, the estimated production of the aquifer at the Thomazo River site during the "wet" season is $2.9 \cdot 10^6$ liters.

$$V \times \varphi \times E = P \qquad (7)$$

where V is a volume of the aquifer in liters;

φ is an effective porosity of a rock constituent the aquifer;

E is a groundwater extraction capacity as a percentage;

P is production potential of the aquifer in liters

The time-lapse ERT interpretation showed that the change in groundwater content between dry and "rainy" seasons is about 15%. During the dry season the amount of groundwater would be 15% less compared to that during the wet season. It leads to the value of effective porosity of the aquifer equal to 50% in the dry season. Consequently, according to formula 7 we obtain that the estimated production of the aquifer during the dry season is $2.45 \cdot 10^6$ liters·

It is important to mention that the formula used to calculate the potential water supply does not take into account the groundwater recharge factor. It is important to have a good evaluation of the groundwater recharge potential because the pumping speed of the groundwater is dependent on it. In addition, the resistivity data collected in December 2010 in order to evaluate the subsurface resistivity distribution typical for a wet season might not fully represent the actual wet season conditions. The wet season in Saint Lucia usually lasts from May until November. Because of the large amount of precipitation during November 2010 we assume that the data collected in December 2010 are more closely related to the "wet" season rather than to the dry season conditions. In addition, the two dimensional ERT survey provides only information about the thickness and the width of the lens body. The lens could have a long extension along the dimension parallel to the Thomazo River. That would increase the volume of the aquifer significantly.

Conclusion

The time-lapse analysis of the two ERT data sets collected during dry and rainy seasons identified the presence of a possibly productive aquifer at the Thomazo River site. The analysis of the 1D IP data confirmed the good quality of the aquifer showing that little or no clay is present in the aquifer. The current study showed that the employment of the two-dimensional ERT survey in a time-lapse mode is capable of providing a good estimation of the groundwater content in the aquifer. This aspect is especially important for the regions with pronounced seasonal variations in the amount of precipitations such as in Saint Lucia. The ratio of the two inversion models provides an

opportunity to directly evaluate the change in groundwater content between dry and rainy seasons

In addition, it has been shown that for the successful detection of a productive aquifer when difficult geological and topographical conditions are present, thorough site pre-selection becomes a crucial step in the successful discovery of a new underground water source.

References

Abu-Shariah, M.I.I., Determination of cave geometry by using a geoelectrical resistivity inverse model, Engineering Geology 105, 2009

Archie G., Electrical Resistivity Log as an Aid in Determining Some Reservoir Characteristics, Transaction of AIME, 1942

AXYS Feasibility Study of Harrison's Cave and Associates Sites, report, AXYS Environmental Consulting, 2000

Beard L.P., Morgan F.D., Assessment of 2D resistivity structure using 1D inversion, Geophysics, 56(6), 1991

Binley A., Kemna A., DC resistivity and induced polarization methods, Hydrogeophysics, p. 129–156, Springer, 2005

Cassiani G., Bruno V., Villa A., Fusi N., Binley A. M., A saline trace test monitored via time-lapse surface electrical resistivity tomography, Journal of Applied Geophysics, 59, 2006

Cardarelli E., Marrone C., Orlando L., Evaluation of tunnel stability using integrated geophysical methods, Journal of Applied Geophysics, 52, 2003

Chilton P.J, Vlugman A.A., Headley J. Groundwater quality monitoring tailored for pollution risk assessment in Barbados, Proceedings MTM-III-Pollution risk assessment in groundwater, 2000

Day M., Doline morphology and development in Barbados, Annals of the Association of American Geographers, 73(2), 1983

Daily W, Ramirez A., LaBrecque D., Nitao J., Electrical Resistivity Tomography of Vadose Water Movement, Water resources research, vol. 28(5), 1992

Daily, W., Ramirez A., Binley A., Remote monitoring of leaks in storage tanks using electrical resistance tomography: Application at the Hanford Site, J. Environ. Eng. Geophys., 9, 11–24, 2004

Donovan S.K., The geology of Barbados: a field guide, Caribbean Journal of Earth Science, 38, 2005

Friedel S., Thielen A., Springman S.M., Investigation of a slope endangered by rainfall-induced landslides using 3D resistivity tomography and geotechnical testing, Journal of Applied Geophysics 60, 2006

Gelis L., Potential of electrical resistivity tomography to detect fault zones in limestone and argillaceous formations in the experimental platform of Tournemire, France, Pure and Applied. Geophysics, 167, 2010

Godio A., Bottino G., Electrical and electromagnetic investigation for landslide characterization

Hack R., Geophysics for slope stability, Surveys in Geophysics, 21, 2000

Hallenburg J.K., Geophysical logging for mineral and engineering applications, PennWell Publishing Co.: Tulsa, 1984

Hobbs H.H., A study of environmental factors in Harrison's cave, Barbados, West Indies, NSF Report, 1994

Kemna A., Vanderborght J., Kulessa B., Vereecken H., Imaging and characterisation of subsurface solute transport using electrical resistivity tomography (ERT) and equivalent transport models, Journal of Hydrology, 267, 2002

Kim J., Yi M., Park S., Kim J.G., 4-D inversion of DC resistivity monitoring data acquired over a dynamically changing earth model, Journal of Applied Geophysics, 68, 2009

LaBrecque, D. J., Yang X., Difference inversion of ERT data: A fast inversion method for 3-D in situ monitoring: Journal of Environmental and Engineering Geophysics, 6, 2001

Lapenna V. et al., High-resolution geoelectrical tomographies in the study of Giarrossa landslide (southern Italy), Bulletin of Engineering Geology and the Environment, 62(3), 2003

Lazzari M., Loperte A., Perrone A., Near surface geophysics techniques and geomorphological approach to reconstruct the hazard cave map in historical and urban areas, Advances in Geosciences, 24, 2010

Lebourg T. et al., Landslides triggered factors analysed by time lapse electrical survey and multidimensional statistical approach, Engineering Geology, 114(3-4), 2010

Lesmes D.P., Frye K.M., Influence of pore fluid chemistry on the complex conductivity and induced polarization responses of Berea sandstone, Journal of Geophysical Research, 106(b3), 2001

Leucci G., Giorgi L., Integrated geophysical surveys to assess the structural conditions of a karstic cave of archaeological importance, Natural Hazards and Earth Systems Sciences, 5, 2005

Loke M.H., Time-lapse resistivity imaging inversion, Proceedings of the 5th Meeting of the Environmental and Engineering Society European Section, 1999

Macdonald R., Hawkesworth C.J., and Heath E., The Lesser Antilles volcanic chain: a study in arc magmatism, Earth-Science Reviews Volume 49, Issues 1-4, 2000

Madden T.R., Transmission system and network analogies to geophysical forward and inverse problems, ONR Technical report, 72(3), 1972

Madden T.R., Swift C.M., Magnetotelluric studies of the electrical conductivity structure of the crust and upper mantle, in the earth's crust and upper mantle, Geophys. Mono. 13, Am. Geophys. Union, 1969

Maury R.C., Westbrook G. K., Baker P. E., Bouysse P, and Westercamp D., Geology of the Lesser Antilles, in Dengo, G. and J. E. Case, eds., The Caribbean region: Boulder, Colorado, Geological Society of America, The Geology of North America, 1990

Mesolella K.J., Sealy H.A., Mahhews R.K., Facies geometries within pleistocene reefs of Barbados, West Indies, The American Association of Petroleum Geologists Bulletin, 54(10), 1970

Miller C.R,, Routh P.S., Brosten T.R., and McNamara J.P., Application of time-lapse ERT imaging to watershed characterization, Geophysics, vol. 73(3), 2008

Morgan F.D., Options for enhancing the water resources of the Fond D'Or watershed, St. Lucia, report, 2009

Morgan F.D., Coles D., Minsley B., Sustainability of the Harrison's Cave System, Barbados: Science, Engineering, and Monitoring, Report to Environmental Special Projects Unit, Government of Barbados, 2007

Morgan F.D., Analysis for the sustainability of the water resources and supply of the Vieux Fort region of St. Lucia, report, 2004

Morgan F.D. Wharton, A.E, Preliminary geophysical imaging of the Harrison's cave system, Barbados, Barbados National Conservation Commission & The University of the West Indies Centre for Environment and Development, 1996

Niesner E., Weidinger J.T., Investigation of a historic and recent landslide area in Ultrahelvetic sediments at the northern boundary of the Alps (Austria) by ERT measurements, The Leading Edge, 27(11), 2008

Nyquist J.E., Peake J.S., Roth M., Comparison of an optimized resistivity array with dipole-dipole soundings in karst terrain, Geophysics, 72(4), 2007

Oldenborger, G.A., Knoll M.D., Routh P.S., LaBrecque D.J., Time-lapse ERT monitoring of an injection/withdrawal experiment in a shallow unconfined aquifer, Geophysics, 72(4), 2007

Oldenborger, G.A., Routh P.S., Knoll M.D., Sensitivity of electrical resistivity tomography data to electrode position errors: Geophysical Journal International, 163, 2005

Oldenburg D.W., Li Y., Estimating depth of investigation in dc resistivity and IP surveys, Geophysics, 64(2), 1999

Panek T., Gravitationally induced caves and other discontinuities detected by 2D electrical resistivity tomography: Case studies from the Polish Flysch Carpathians, Geomorphology, 123, 2010

Roth M.J.S., Mackey J.R., Mackey C., Nyquist J.E., A case study of the reliability of multielectrode earth resistivity testing for geotechnical investigations in karst terrains, Engineering Geology 65, 2002

Taylor F.W., Mann P., Late quaternary folding of coral reef terraces, Barbados, Geology, 19, 1991

Saint Lucia natural resources and agricultural development project: Studies and proposals for the implementation of a land registration program, 1986

Shi W., Advanced modeling and inversion techniques for three-dimensional geoelectrical surveys, PhD Thesis, 1998

Slater L.D., David Lesmes D., IP interpretation in environmental investigations, Geophysics, 67(1), 2002

Slater L.D., Sandberg S.K., Resistivity and induced polarization monitoring of salt transport under natural hydraulic gradients: Geophysics, 65, 2000

Suzuki, K., Higashi, S., Groundwater flow after heavy rain in landslide-slope area from 2-D inversion of resistivity monitoring data, Geophysics 66 (3), 2001

Szalai S. et al., Geoelectric mapping of near-surface karstic fractures by using null arrays, Geophysics, 67(6), 2002

Telford W.M., Geldart L. P., and Sheriff R. E., Applied geophysics, 2nd ed.: Cambridge University Press, 1990

Valois R. et al., Karstic morphologies identified with geophysics around Saulges Caves (Mayenne,France), Archaeological Prospection, 17, 2010

Ward S. H., Geotechnical and environmental geophysics, SEG, 1990

Zhang, J., Mackie, R.L., Madden, T.R., Three-dimensional resistivity forward modeling and inversion using conjugate gradients, Geophysics, 60, 1995